

# Excited-State Tautomerization in the 7-Azaindole-(H<sub>2</sub>O)<sub>n</sub> (*n* = 1 and 2) Complexes in the Gas Phase and in Solution: A Theoretical Study

Hua Fang and Yongho Kim\*

Department of Chemistry, Kyung Hee University, 1 Seochun-Dong, Giheung-Gu, Yongin-Si, Gyeonggi-Do, 446-701, Korea

Supporting Information

**ABSTRACT:** A systematic study of the excited-state tautomerization of 7-azaindole-(H<sub>2</sub>O)<sub>n</sub> (*n* = 1 and 2) complexes in both gas and solution phases were investigated theoretically. Electronic structures and energies for the reactant, transition state (TS), and product were computed using the time-dependent density functional theory (TDDFT) and complete active space self-consistent field (CASSCF) levels with 6-31G(d,p), 6-311G(d,p), and 6-311+G(d,p) basis sets. Barrier heights and tautomerization energies were corrected by the second-order multireference perturbation theory (MRPT2) to consider the dynamic electron correlation. The solvent effect decreased the tautomerization barrier height in the 7-azaindole-H<sub>2</sub>O complex. In the 7-azaindole-(H<sub>2</sub>O)<sub>2</sub> complex, two transition states were found for two asynchronous but concerted paths: in the first, the pyrrole ring proton moved first to water; in the second, the water proton moved first to the pyridine ring. The CASSCF level with the MRPT2 correction clearly showed that the former path was much preferable to the latter. The preferable barrier height was only 1.6 kcal/mol with a zero-point energy correction, which would make the excited-state tautomerization possible. At all TDDFT levels, the TS structures and barrier heights depended on both the basis set used and the solvent effect. Most TDDFT methods failed to reproduce the CASSCF structures and MRPT2 energies. Only two methods, WB97XD/6-31G(d,p) and M062X/6-311+G(d,p), predicted two TSs for the two asynchronous paths in the 7AI-(H<sub>2</sub>O)<sub>2</sub> complex but failed to reproduce the energetics. Further systematic study is necessary to test whether current TDDFT methods, including solvent effects, can be used to understand excited-state proton transfer reactions.

## 1. INTRODUCTION

Proton/hydrogen-atom transfer reactions have attracted much attention due to their importance for understanding many physical, chemical, and biological phenomena.<sup>1</sup> The characterization of the nature of the proton or hydrogen atom transfer process is of great importance not only from the point of view of spectroscopy but also from the point of view of reaction dynamics. Among many molecules, 7-azaindole (7AI) is an important model system for the study of excited state proton transfer processes since it resembles molecules of the DNA base pair.<sup>2</sup> 7AI contains one proton donor and one proton acceptor and thereby displays simple hydrogen-bonding structures upon dimerization and complexation with solvents. Therefore, the 7AI-dimer and 7AI hydrogen-bonded clusters have been studied extensively.

In an early theoretical calculation, Chaban and Gordon,<sup>3,4</sup> studied the tautomerization reaction of 7AI and a 1:1 7AI-H<sub>2</sub>O complex (7AI-H<sub>2</sub>O) in the singlet ground (S<sub>0</sub>) and first excited (S<sub>1</sub>) states. They used the complete active space self-consistent field (CASSCF) method with multireference second-order perturbation theory (MCQDPT2),<sup>5</sup> which included dynamic electron correlation to calculate energies and intrinsic reaction coordinates for the proton transfer process. They found that the normal 7AI form was more stable than the tautomer in the S<sub>0</sub> state, whereas the relative energies were reversed in the S<sub>1</sub> state. The activation energy for tautomerization in 7AI was dramatically reduced by complexation with one water molecule when the dynamic electron correlation was considered. Casadesús et al.<sup>6</sup>

investigated the tautomerization of 7AI-(H<sub>2</sub>O)<sub>n</sub> (*n* = 0 – 4) in the S<sub>1</sub> state. The geometries were optimized using the single-excitation configuration interaction (CIS) method, and the energies were calculated at the time-dependent density functional theory (TDDFT) level. The dependence of activation barriers on the number of attached water molecules was discussed.

Fernández-Ramos et al.<sup>7</sup> calculated the rate constant for the excited state hydrogen transfer reaction of 7AI–water complexes in solution using the Onsager model. They concluded that concerted proton tunneling rate constants dominated the tautomerization process. However, their transition state (TS) structures, which were calculated at the CASSCF(8,8)/6-31G(d) level, were very different from those obtained from previous higher-level calculations.<sup>4</sup> Deviation of the structural parameters in the TS was more than 0.2 Å (see Table 1). Otherwise, the barrier height in the 1:1 7AI/H<sub>2</sub>O complex at the CASSCF(8,8)/6-31G(d) level was 20.64 kcal/mol,<sup>7</sup> whereas the barrier height at the CASSCF(10,9)/DZP level was 18.20 kcal/mol.<sup>4</sup> For the two-waters complex (the only one that can be directly compared with experimental data), the calculations indicated a concerted, though nonsynchronous, reaction path with a high-energy barrier at 16.94 kcal/mol.<sup>7</sup> Recently, Kina et al.<sup>8</sup> conducted *ab initio* QM/MM molecular dynamics (AIMD) simulations for the excited-state full tautomerization process in 7AI-(H<sub>2</sub>O)<sub>n</sub> (*n* = 1, 2)

Received: November 10, 2010

Published: January 19, 2011

**Table 1.** Geometric Parameters of Reactant, Product, and Transition States for Excited-State Proton Transfer in 7Al–H<sub>2</sub>O Complexes<sup>a</sup>

computational method	reactant		product	
	<i>r</i> (H <sub>10</sub> –O <sub>16</sub> )	<i>r</i> (H <sub>17</sub> –N <sub>6</sub> )	<i>r</i> (N <sub>1</sub> –H <sub>10</sub> )	<i>r</i> (O <sub>16</sub> –H <sub>17</sub> )
CIS/6-31G(d) <sup>b</sup>	2.09	2.05	2.17	2.21
RICC2/TZVP <sup>c</sup>	1.781	1.795	1.990	1.986
CASSCF(8,8)/6-31G(d,p) <sup>d</sup>	2.166	2.131	2.182	2.196
CASSCF(10,9)/6-31G(d,p) <sup>e</sup>	2.136	2.126	2.190	2.196
CASSCF(10,9)/6-311G(d,p)	2.141	2.135	2.206	2.172
CASSCF(10,9)/DZP <sup>f</sup>	2.164	2.125	2.199	2.192
B3LYP/6-31G(d,p)	1.823	1.823	1.969	1.979
B3LYP/6-311+G(d,p)	1.890	1.831	1.963	2.052
CAM-B3LYP/6-31G(d,p)	1.794	1.808	1.958	1.950
CAM-B3LYP/6-311+G(d,p)	1.868	1.818	1.951	2.013
LC-BLYP/6-31G(d,p)	1.773	1.797	1.936	1.912
LC-BLYP/6-311+G(d,p)	1.843	1.803	1.924	1.965
M062X/6-31G(d,p)	1.821	1.836	2.006	1.970
M062X/6-311+G(d,p)	1.877	1.855	1.987	1.995
WB97XD/6-31G(d,p)	1.827	1.842	1.988	1.968
WB97XD/6-311+G(d,p)	1.889	1.843	1.973	2.022
exp. <sup>g</sup>	1.950	2.117		
transition state				
	<i>r</i> (N <sub>1</sub> –H <sub>10</sub> )	<i>r</i> (H <sub>10</sub> –O <sub>16</sub> )	<i>r</i> (O <sub>16</sub> –H <sub>17</sub> )	<i>r</i> (H <sub>17</sub> –N <sub>6</sub> )
CIS/6-31G(d) <sup>b</sup>	1.30	1.22	1.27	1.26
CASSCF(8,8)/6-31G(d) <sup>d</sup>	1.101	1.484	1.269	1.237
CASSCF(10,9)/6-31G(d,p) <sup>e</sup>	1.258	1.220	1.086	1.444
CASSCF(10,9)/6-311G(d,p)	1.277	1.198	1.067	1.479
CASSCF(10,9)/DZP <sup>f</sup>	1.263	1.213	1.084	1.447
B3LYP/6-31G(d,p)	1.224	1.296	1.168	1.357
B3LYP/6-311+G(d,p)	1.151	1.407	1.264	1.253
CAM-B3LYP/6-31G(d,p)	1.221	1.289	1.151	1.369
CAM-B3LYP/6-311+G(d,p)	1.172	1.359	1.226	1.282
LC-BLYP/6-31G(d,p)	1.223	1.277	1.140	1.377
LC-BLYP/6-311+G(d,p)	1.183	1.333	1.210	1.292
M062X/6-31G(d,p)	1.233	1.272	1.123	1.408
M062X/6-311+G(d,p)	1.234	1.270	1.143	1.379
WB97XD/6-31G(d,p)	1.224	1.282	1.153	1.362
WB97XD/6-311+G(d,p)	1.176	1.349	1.220	1.283

<sup>a</sup> Bond distances are in Å. <sup>b</sup> Ref 6. <sup>c</sup> Ref 41. <sup>d</sup> Ref 7. <sup>e</sup> Ref 42. <sup>f</sup> Ref 4. <sup>g</sup> Ref 16. The structural parameters are obtained from the fit to the experimental rotational constants.

complexes in gas and water. They found that the ESDPT takes place asynchronously in both the gas and solution phases.

The excited-state tautomerization in 7Al has been observed in the condensed phase in alcohol or water solutions.<sup>9–11</sup> Although the tautomerization occurs very rapidly in aqueous solution, the excited-state multiple-proton transfer reactions in the 7Al–(H<sub>2</sub>O)<sub>n</sub> (*n* = 1, 2) complexes in the gas phase have been uncertain. Huang et al.<sup>12</sup> studied the 1:1 7Al/water complex in the first excited state in cold beams and reported a fluorescence lifetime of 8 ns, which implies that the tautomerization rate constant of ESDPT cannot be larger than approximately 10<sup>7</sup> s<sup>-1</sup>. However, no direct observation of ESDPT in this complex has yet been made. Folmer et al.<sup>13</sup> observed very fast decay profiles of the femtosecond pump–probe transients of 7Al–(H<sub>2</sub>O)<sub>n</sub> (*n* =

2–4) complexes and ascribed them to the excited-state multiple-proton transfer. However, the fast decay time constants did not agree with those predicted from a very sharp bandwidth of jet-cooled fluorescence excitation spectra<sup>14</sup> and the dispersed fluorescence spectra of 7Al–(H<sub>2</sub>O)<sub>n</sub> (*n* = 1 – 3) complexes.<sup>15</sup> Schmitt et al.<sup>16</sup> measured the rotationally resolved electronic spectra of the 7Al–(H<sub>2</sub>O)<sub>n</sub> (*n* = 1, 2) clusters in a molecular beam. From the rotational constants, the structures in the S<sub>0</sub> and S<sub>1</sub> electronic states were determined. They also predicted the long lifetime of the excited species from the narrow bandwidth, which suggested no excited-state tautomerization in the gas phase.

However, Sakota et al.<sup>17</sup> recently investigated the excited-state multiple-proton transfer reactions in 7Al water clusters,

**Table 2.** Geometric Parameters of Reactant, Product, and Transition States for Excited-State Proton Transfer in 7AI-(H<sub>2</sub>O)<sub>2</sub> Complexes<sup>a</sup>

computational method	reactant			product		
	r(H <sub>10</sub> -O <sub>16</sub> )	r(O <sub>20</sub> -H <sub>17</sub> )	r(H <sub>19</sub> -N <sub>6</sub> )	r(N <sub>1</sub> -H <sub>10</sub> )	r(O <sub>16</sub> -H <sub>17</sub> )	r(O <sub>20</sub> -H <sub>19</sub> )
CIS/6-31G(d) <sup>b</sup>	1.79	1.75	1.84	1.77		
RICC2/TZVP <sup>c</sup>	1.621	1.638	1.676	1.863	1.753	1.808
CASSCF(8,8)/6-31G(d) <sup>d</sup>	1.978	1.894	2.013	2.064	1.915	2.021
CASSCF(10,9)/6-31G(d,p)	1.792	1.809	1.881	2.065	1.919	2.010
CASSCF(10,9)/6-311G(d,p)	1.796	1.822	1.895	2.078	1.930	2.015
B3LYP/6-31G(d,p)	1.652	1.638	1.683	1.824	1.733	1.798
B3LYP/6-311+G(d,p)	1.726	1.686	1.706	1.834	1.773	1.868
CAM-B3LYP/6-31G(d,p)	1.623	1.612	1.669	1.815	1.711	1.776
CAM-B3LYP/6-311+G(d,p)	1.698	1.662	1.693	1.822	1.749	1.840
LC-BLYP/6-31G(d,p)	1.592	1.578	1.650	1.792	1.675	1.742
LC-BLYP/6-311+G(d,p)	1.672	1.631	1.674	1.795	1.711	1.801
M062X/6-31G(d,p)	1.578	1.582	1.643	1.843	1.735	1.786
M062X/6-311+G(d,p)	1.696	1.680	1.708	1.860	1.780	1.849
WB97XD/6-31G(d,p)	1.651	1.653	1.703	1.833	1.742	1.789
WB97XD/6-311+G(d,p)	1.708	1.688	1.717	1.834	1.768	1.836
exp. <sup>e</sup>	1.693	1.679	1.818			
transition state						
	r(N <sub>1</sub> -H <sub>10</sub> )	r(H <sub>10</sub> -O <sub>16</sub> )	r(O <sub>16</sub> -H <sub>17</sub> )	r(H <sub>17</sub> -O <sub>20</sub> )	r(O <sub>20</sub> -H <sub>19</sub> )	r(H <sub>19</sub> -N <sub>6</sub> )
CIS/6-31G(d) <sup>b</sup>	1.22	1.28	1.25	1.19	1.34	1.19
CASSCF(8,8)/6-31G(d) <sup>d</sup>	1.056	1.580	1.032	1.462	1.379	1.130
CASSCF(10,9)/6-31G(d,p) TS1	1.394	1.101	1.079	1.329	1.050	1.493
CASSCF(10,9)/6-311G(d,p) TS1	1.431	1.079	1.072	1.335	1.036	1.525
CASSCF(10,9)/6-31G(d,p) TS2	1.088	1.464	1.061	1.372	1.351	1.141
CASSCF(10,9)/6-311G(d,p) TS2	1.075	1.496	1.044	1.401	1.392	1.117
B3LYP/6-31G(d,p)	1.204	1.299	1.147	1.285	1.201	1.292
B3LYP/6-311+G(d,p)	1.123	1.428	1.122	1.314	1.312	1.191
CAM-B3LYP/6-31G(d,p)	1.209	1.281	1.138	1.283	1.178	1.309
CAM-B3LYP/6-311+G(d,p)	1.128	1.406	1.117	1.309	1.288	1.201
LC-BLYP/6-31G(d,p)	1.217	1.264	1.133	1.278	1.156	1.330
LC-BLYP/6-311+G(d,p)	1.139	1.378	1.121	1.293	1.264	1.216
M062X/6-31G(d,p)	1.248	1.236	1.126	1.293	1.126	1.375
M062X/6-311+G(d,p)	1.219	1.267	1.131	1.280	1.174	1.309
WB97XD/6-31G(d,p)	1.213	1.272	1.139	1.280	1.182	1.298
WB97XD/6-311+G(d,p)	1.129	1.400	1.117	1.306	1.301	1.188

<sup>a</sup> Bond distances are in Å. <sup>b</sup> Ref 6. <sup>c</sup> Ref 41. <sup>d</sup> Ref 7. <sup>e</sup> Ref 16. The structural parameters are obtained from the fit to the experimental rotational constants.

7AI-(H<sub>2</sub>O)<sub>n</sub> ( $n = 2, 3$ ), in the gas phase by combining electronic spectroscopy and quantum chemical calculations. They found that the 7AI-(H<sub>2</sub>O)<sub>2</sub> and 7AI-(CH<sub>3</sub>OH)<sub>2</sub> geometries were similar; the solvent molecules bridged the heteroaromatic N atom and the NH hydrogen by intermolecular hydrogen bonds, forming a cyclic structure.<sup>14,18</sup> Most importantly, they successfully observed the tautomer of the 7AI-(H<sub>2</sub>O)<sub>2</sub> complex in the excited state and showed that the ESTPT occurs in the gas phase.

However, there are no theoretical calculations for the excited-state proton transfer in 7AI-(H<sub>2</sub>O)<sub>2</sub> complexes using the TDDFT method. Currently, the most widely used method to describe the excited states of molecules is the linear-response time-dependent density functional theory.<sup>19,20</sup> Since TDDFT is computationally efficient for excited-state calculations, a large number of excited-state properties based on the TDDFT method

have been performed. TDDFT yielded surprisingly accurate absorption spectra.<sup>21,22</sup> However, dramatic failures of the TDDFT method have also been recently found. For example, Ryberg states are not appropriately described due to the rapid asymptotic decay of standard exchange-correlation functionals;<sup>23</sup> doubly excited states are not contained owing to the linear-response formalism of TDDFT,<sup>24–26</sup> and charge-transfer excited states are given lower excitation energies with the incorrect asymptotic potential energy surfaces because of spurious electron-transfer self-interaction.<sup>27–30</sup>

The purpose of this work was to perform a systematic study of proton transfer in the biologically interesting 7AI-H<sub>2</sub>O and 7AI-(H<sub>2</sub>O)<sub>2</sub> complexes. The main interest was to determine if the TDDFT method could fit the excited state chemical reaction. In this study, five TDDFT methods, which contained hybrid

functional, long-rang correction (LC) and empirical dispersion functionals, were used to systematically investigate the tautomerization reaction in the  $S_1$  state in both the gas and solution phases. To avoid possible TDDFT artifacts, the multiconfigurational CASSCF method was used to assess TDDFT reliability in the present study.

## 2. COMPUTATIONAL METHODS

Reactant, product, and TS geometries of the excited state tautomerization in the 7AI–( $H_2O$ ) $_n$  ( $n = 1$  and 2) complexes were fully optimized at the TDDFT and CASSCF level with 6-31G(d,p), 6-311G(d,p), and 6-311+G(d,p) basis sets using the Gaussian 09 program<sup>31</sup> in the gas phase and in solution. The crucial step to conduct the CASSCF calculation was to select the proper active space. The obvious choice for an active space in 7AI complexes would include four  $\pi$  bonds, four corresponding antibonding orbitals, and one nitrogen lone pair, resulting in an active space of 10 electrons in nine orbitals, which was denoted as CASSCF(10,9). Calculating vibrational frequencies and establishing no imaginary frequency for the reactant and product and one imaginary frequency for the TS verified optimized structures. Single point energy calculations were also performed using the second-order multireference perturbation theory (MRPT2) for stationary points. All MRPT2 calculations were performed using the GAMESS program.<sup>32</sup>

Analytic TDDFT gradients were calculated using the variational TDDFT formulation of Furche and Ahlrichs.<sup>33</sup> Several different exchange-correlation DFT potentials were used for the systems. We used Becke's three-parameter Lee–Yang–Parr hybrid functionals,<sup>34</sup> (B3LYP), Handy and co-workers' long-range corrected version of B3LYP using the Coulomb-attenuating method,<sup>35</sup> (CAM-B3LYP), a long-range-corrected version of BLYP<sup>36</sup> (LC-BLYP), the hybrid functional of Truhlar and Zhao<sup>37</sup> (M062X), and the latest functional from Head-Gordon and co-workers, which included empirical dispersion<sup>36</sup> (WB97XD).

We performed polarizable continuum model calculations using the integral equation formalism (IEPCM)<sup>38–40</sup> at the TDDFT and CASSCF levels to investigate the mechanism of tautomerization in water. The geometries of reactant, product, and TS were completely optimized in solution. Currently, the solvent effect is not implemented in the MRPT2 calculations. Therefore, the gas phase MRPT2 energies and the solvation energies at the CASSCF level were used to estimate the MRPT2 energies in water.

## 3. RESULTS AND DISCUSSION

Casadesús et al.<sup>6</sup> examined the reaction path for the tautomerization of the 7AI– $H_2O$  complex in the  $S_1$  state using CIS with the 6-31G(d) basis set. Since CIS theory does not include higher-level electron correlation, which has an important influence on H-bonded structures, CIS does not give very accurate results. Schmitt et al.<sup>41</sup> studied the normal and tautomer forms of 7AI–( $H_2O$ ) $_n$  ( $n = 1, 2$ ) in their ground and two lowest singlet excited states by using the RICC2 method. They found that water complexation of 7AI with one and two water molecules stabilizes the more polar L<sub>a</sub> state, which has been observed experimentally. The CASSCF(10,9)/DZP level was the highest level reported in the literature for the 7AI– $H_2O$  complex.<sup>4</sup> Duong and Kim<sup>42,43</sup> studied the 7AI– $H_2O$  complex at the CASSCF(10,9)/6-31G(d,p) level and showed that the geometries of the reactant, product, and TS were in good agreement with

previous studies at the CASSCF(10,9)/DZP level.<sup>4,8</sup> The geometry of the bare 7AI molecule<sup>4</sup> is mostly unaffected by complex formation. Therefore, only the geometric parameters describing hydrogen bond (H-bond) distances are given in Tables 1 and 2. Although no excited-state tautomerization was observed for the 1:1 complex in the gas phase, Sakota et al.<sup>17</sup> suggested that tautomerization occurs via excited-state triple proton transfer in the cyclic 1:2 complex. Therefore, it is interesting to make a systematic comparison of the structures and energies of the excited-state tautomerization between 1:1 and 1:2 complexes of 7AI with  $H_2O$ . In this study, structures of the reactant, TS, and product were obtained by TDDFT and CASSCF methods using various basis sets. To test whether the DFT functional could correctly predict stationary points of the 7AI– $H_2O$  complex in the excited-state tautomerization, the TDDFT and CASSCF results were compared.

**3.1. 1:1 Complex of 7AI with  $H_2O$  in the Gas Phase.** Structures of the stationary points in the 1:1 7AI complex with water optimized at the CASSCF/6-31G(d,p) level are shown in Figure 1. For the 7AI– $H_2O$  complex, the H-bond distances,  $H_{10}$ – $O_{16}$  and  $H_{17}$ – $N_6$  in the reactant and  $N_1$ – $H_{10}$  and  $O_{16}$ – $H_{17}$  in the product at the B3LYP level using the 6-31G(d,p) basis set were 0.313 Å, 0.303 Å, 0.221 Å, and 0.217 Å shorter than those at the CASSCF level, respectively (Table 1). The shorter the H-bond length, the higher the H-bond energy; therefore the B3LYP level predicted strong H bonds compared to the CASSCF results. The hybrid M062X functional gave similar results to the B3LYP analysis. The H-bond distances,  $H_{10}$ – $O_{16}$  and  $H_{17}$ – $N_6$  in the reactant and  $N_1$ – $H_{10}$  and  $O_{16}$ – $H_{17}$  in the product, were underestimated by 0.315 Å, 0.290 Å, 0.184 Å, and 0.226 Å, respectively, compared with corresponding CASSCF values. When the long-range corrected functionals (CAM-B3LYP and LC-BLYP) were used, the H-bond distances,  $H_{10}$ – $O_{16}$  and  $H_{17}$ – $N_6$  in the reactant and  $N_1$ – $H_{10}$  and  $O_{16}$ – $H_{17}$  in the product, were on average 0.353 Å, 0.324 Å, 0.243 Å, and 0.265 Å shorter than the corresponding CASSCF values, respectively. The long-range corrected functionals predicted slightly shorter H-bond distances than in B3LYP or M062X. The WB97XD functional that included empirical dispersion was also used in the 7AI– $H_2O$  complex. Compared to the CASSCF(10,9)/6-31G(d,p) results, the H-bond distances  $H_{10}$ – $O_{16}$  and  $H_{17}$ – $N_6$  in the reactant and  $N_1$ – $H_{10}$  and  $O_{16}$ – $H_{17}$  in the product were underestimated by 0.309 Å, 0.284 Å, 0.202 Å, and 0.228 Å, respectively. Among the DFT methods used in this study, the long-range corrected functionals predicted the shortest H-bond distances (the highest H-bond energies) in the reactant and product 7AI– $H_2O$  complex. When the larger 6-311+G(d,p) basis set was used, all H-bond distances except  $N_1$ – $H_{10}$  of the product became larger at all DFT levels, although they are still shorter than the CASSCF values.

Schmitt et al.<sup>16</sup> measured the rotationally resolved electronic spectra of the 7AI–( $H_2O$ ) $_n$  ( $n = 1, 2$ ) clusters in a molecular beam and obtained the geometry parameters from the fit to the experimental rotational constants. The comparison to calculated CASSCF(10,9) results shows that the  $H_{17}$ – $N_6$  distance in the reactant at the CASSCF(10,9)/6-31G(d,p) (or CASSCF(10,9)/6-311G(d,p)) level is consistent with the experimental value, and the  $H_{10}$ – $O_{16}$  distance at the CASSCF(10,9) level is longer than the experimental value.

TS geometries for the excited-state tautomerization in 7AI– $H_2O$  were fully optimized and confirmed by frequency

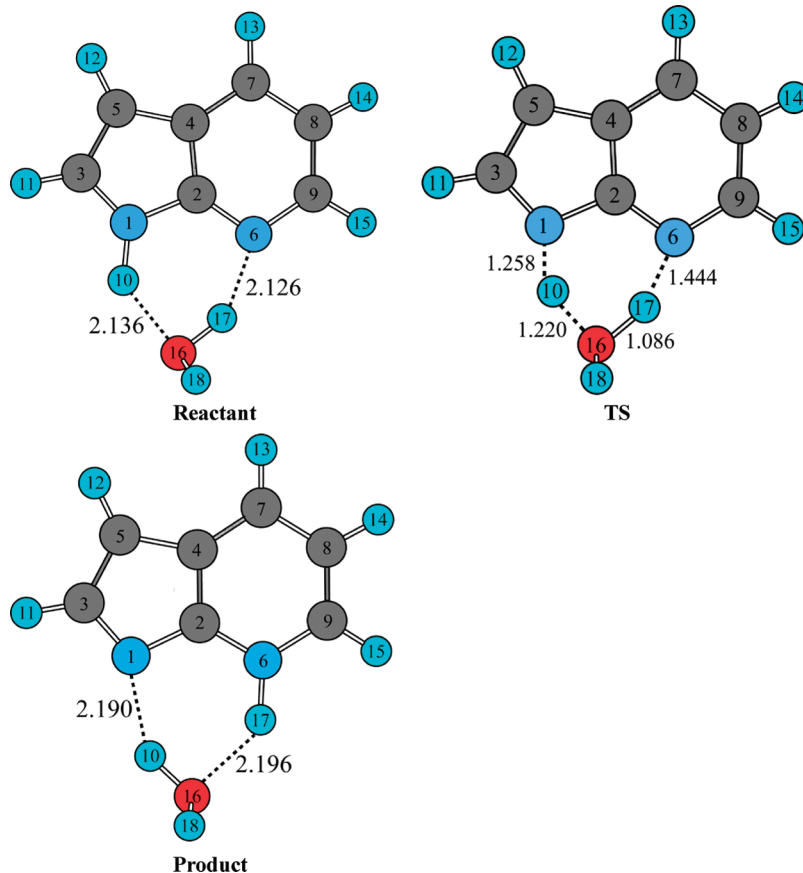


**Figure 1.** Excited-state structures of the reactant, TS, and product for excited-state proton transfer in the 7AI–H<sub>2</sub>O complex.

calculations, with some of the geometric parameters listed in Table 1. The ESDPT potential energy curves in the 7AI–H<sub>2</sub>O complex were studied at the MRPT2/CASSCF(10,9)/6-31G(d, p) level. It was shown that two protons were transferred asynchronously, but concertedly. In the 7AI–H<sub>2</sub>O TS at the CASSCF level, the H<sub>10</sub> atom moved more than halfway along the reaction coordinate toward O<sub>16</sub> (Figure 1), whereas the H<sub>17</sub> atom rarely moved. In this asynchronous double proton transfer, the H<sub>10</sub> atom moved first, followed by the H<sub>17</sub> atom. However, in the TSs at the various TDDFT levels using the same basis sets, the H<sub>10</sub> atom moved slightly less than halfway along the reaction coordinate, and the H<sub>17</sub> atom moved slightly more than at the CASSCF level. All of the TS structures at the TDDFT/6-31G(d, p) level seemed to satisfy Hammond's postulate that the TS of the exothermic reaction resembles the reactant structure (denoted as an early TS), although the position of the two H atoms at the TS was not completely synchronized. When the 6-311+G(d,p) basis set was used, all TDDFT methods except M062X predicted completely different TS structures, in which the H<sub>17</sub> atom moved about halfway along the reaction coordinate toward N<sub>6</sub>, whereas the H<sub>10</sub> atom moved very little. In this case, the H<sub>17</sub> atom moved first followed by the H<sub>10</sub> atom. The use of a larger 6-311+G(d,p) basis set resulted in a different asynchronous mechanism with the opposite order of proton transfer. This TS structure is similar to one reported previously at the CASSCF(8,8)/6-31G(d,p) level. It is interesting to note that the M062X method, unlike other TDDFT methods, predicted consistent TS structures irrespective of the basis set size.

A correlation plot using H-bond distances can be used to visualize hydrogen bond characteristics and proton transfer transition states. Limbach et al.<sup>44–46</sup> defined the natural hydrogen bond coordinates  $q_1 = 1/2(r_{\text{AH}} - r_{\text{BH}})$  and  $q_2 = r_{\text{AH}} + r_{\text{BH}}$  to represent the correlation between  $r_{\text{AH}}$  and  $r_{\text{BH}}$  in many hydrogen-bonded complexes (A–H···B). For a linear H bond,  $q_1$  represents the dislocation of H from the H-bond center, and  $q_2$  represents the distance between the two heavy atoms. A strong H-bond results in short  $r_{\text{BH}}$  and slightly elongated  $r_{\text{AH}}$  distances. Bond distance depends on bond energy and order. Pauling suggested an exponential relationship between valence bond order and bond length. In the A–H···B complexes, the  $r_{\text{AH}}$  and  $r_{\text{BH}}$  distances depend on each other, leading to allowed  $r_{\text{AH}}$  and  $r_{\text{BH}}$  values based on the following Pauling equations under the assumption that the sum of two bond orders is conserved,  $n_{\text{AH}} + n_{\text{BH}} = 1$ :

$$r_{\text{AH}} - r_{\text{AH}}^0 = a_{\text{AH}} \ln n_{\text{AH}} \quad (1)$$

$$r_{\text{BH}} - r_{\text{BH}}^0 = a_{\text{BH}} \ln n_{\text{BH}} \quad (2)$$

where  $r_{\text{AH}}^0$  and  $r_{\text{BH}}^0$  are the equilibrium lengths of the free AH and BH bonds and  $a_{\text{AH}}$  and  $a_{\text{BH}}$  are the parameters describing the decrease of the AH and the HB unit bond valences with the corresponding distances. This type of correlation, which is called the “bond energy bond order method”, has been used for many years to study hydrogen atom transfer.<sup>47,48</sup> When H is transferred from A to B in the A–H···B complex,  $q_1$  increases from

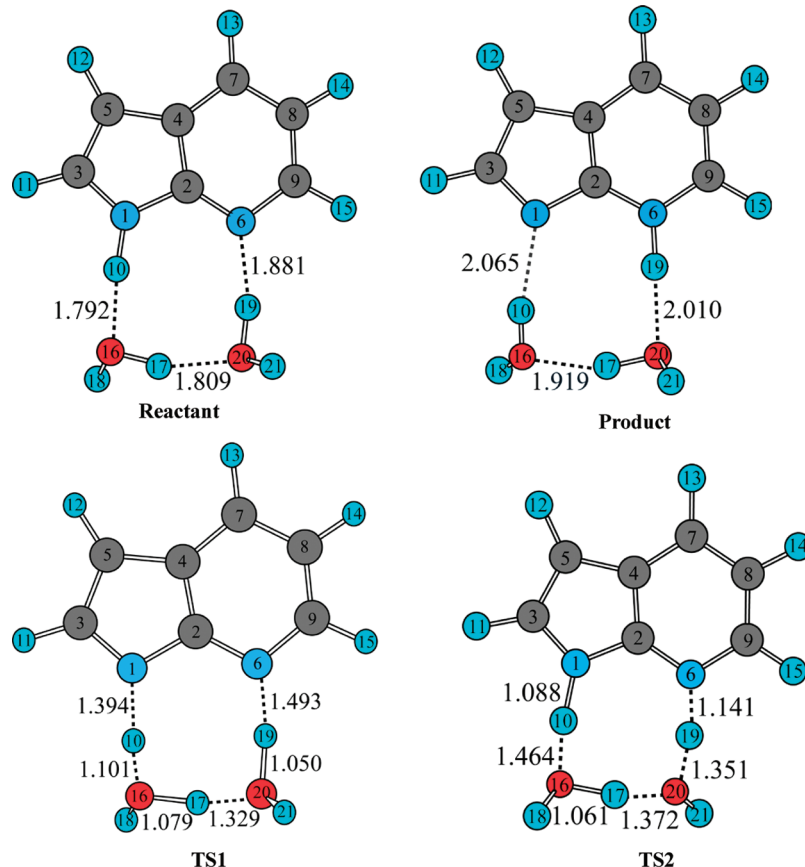


**Figure 2.** Excited-state CASSCF(10,9)/6-31G(d,p) structures of the reactant, product, and TS for asynchronous proton transfer in the 7AI-(H<sub>2</sub>O)<sub>2</sub> complex. In the TS1 structure, H<sub>10</sub> moves first. In the TS2 structure, H<sub>19</sub> moves first.

negative to positive values, and  $q_2$  goes through a minimum, which is located at  $q_1 = 0$ . Limbach et al.<sup>44–46</sup> suggested that both proton transfer and hydrogen-bonding coordinates could be combined into the same correlation. This correlation can be used to study the characteristics of transition state, such as earliness or lateness, bond order, and asynchronicity. The  $q_1$  value of TS is negative or positive when the TS is either early or late, respectively. In addition, the two TS  $q_1$  values for the double proton transfer should be very similar and different in the synchronous and asynchronous mechanism, respectively.

The correlations between N<sub>1</sub>–H<sub>10</sub> and H<sub>10</sub>–O<sub>16</sub> distances (H<sub>10</sub> transfer) and N<sub>6</sub>–H<sub>17</sub> and H<sub>17</sub>–O<sub>16</sub> distances (H<sub>17</sub> transfer) for the 7AI–H<sub>2</sub>O complex are depicted in Figure 3. It is interesting to note that all points for the reactant, product, and TS were very close to the black line regardless of computational level, which suggests that the sum of bond order at all stationary points was approximately conserved. All  $q_2$  values of the reactant and product at the TDDFT level were significantly smaller than the CASSCF values; this is consistent with the fact that TDDFT overestimates H-bond strength, leading to shorter H-bond distances. In the synchronous process, two TS  $q_1$  values for two proton transfers should be approximately the same. These  $q_1$  values for H<sub>10</sub> and H<sub>17</sub> transfer at all TDDFT levels using the 6-31G(d,p) basis set were both negative, consistent with the early TS, but not the same. However, H<sub>10</sub> and H<sub>17</sub> transfer values at the CASSCF/6-31G(d,p) level were slightly positive and very negative, respectively, which resulted from a highly asynchronous TS (slightly late and very early TS in terms of H<sub>10</sub> and H<sub>17</sub> transfers, respectively).

When the 6-311+G(d,p) basis set was used at TDDFT levels, H<sub>10</sub>  $q_2$  and  $q_1$  values for the reactant became significantly larger and smaller, which moved the correlation points ( $q_1$  and  $q_2$ ) toward the upper-left side of Figure 3B, along the black line. For simplicity, the  $q_2$  and  $q_1$  values of H<sub>10</sub> transfer were denoted as “the H<sub>10</sub> correlation point”. The H<sub>17</sub> correlation points for the product also moved to the upper-right side along the black line. Positions of the TS on the H<sub>10</sub> and H<sub>17</sub> transfer reaction coordinates became very early and late, respectively, using larger basis sets. Only the M062X level predicted an almost identical correlation of TS for both H<sub>10</sub> and H<sub>17</sub> transfers; i.e., the locations of TSs were not dependent on the size of basis sets. The blue line represents correlations along the intrinsic reaction coordinate of the ESDPT calculated at the CASSCF(10,9)/6-31G(d,p) level. It is very interesting to note that the blue line is very different in shape from the black lines, which means that the sum of the bond order was not conserved along the intrinsic reaction coordinate. For H<sub>10</sub> transfer, the blue line was always under the black line except at the TS, which indicates that the sum of the bond order was larger than unity at both the reactant- and product-side reaction coordinates. However, for H<sub>17</sub> transfer, the blue line was above the black line near  $q_1 = 0$ , which means that the sum of the bond order was less than unity. It is also very interesting that the blue lines were flat at the bottom near  $q_1 = 0$ , which was attributed to an almost constant  $q_2$  value that is the distance between two end atoms. These results suggest that the end atom distance rarely changed during the proton transfer near  $q_1 = 0$ . This finding was not surprising because it is

**Table 3.** Reaction Energies, Barrier Heights, and Dipole Moments for Proton Transfer in 7Al–H<sub>2</sub>O and 7Al–(H<sub>2</sub>O)<sub>2</sub> in the S<sub>1</sub> State at Various Levels of Theory<sup>a</sup>

computational method	7Al–H <sub>2</sub> O						7Al–(H <sub>2</sub> O) <sub>2</sub>					
				$\mu$ (D)						$\mu$ (D)		
	$\Delta V$ (kcal/mol)	$\Delta E$ (kcal/mol)	R	TS	P	$\Delta V$ (kcal/mol)	$\Delta E$ (kcal/mol)	R	TS	P		
CIS/6-31G(d) <sup>b</sup>	26.94	−18.15				24.35	−15.85					
RICC2/TZVP <sup>c</sup>		−22.51					−20.01					
CASSCF(8,8)/6-31G(d) <sup>d</sup>	20.64(22.07)	−33.19	1.99	5.02	2.06	16.94	−32.45	1.51	6.88	2.21		
CASSCF(10,9)/DZP(d,p) <sup>e</sup>	18.20(14.7)	−31.80(−31.2)										
MCQDPT2/CASSCF(10,9)/DZP <sup>e</sup>	9.80(6.3)	−18.00(−17.4)										
CASSCF(10,9)/6-31G(d,p) <sup>f</sup>	18.08(14.39)	−28.56(−27.92)	1.78	4.28	2.05	15.84(11.04) <sup>g</sup> 15.26(10.72) <sup>h</sup>	−32.23(−32.00)	4.87	5.23 <sup>g</sup> 5.79 <sup>h</sup>	1.92		
CASSCF(10,9)/6-311G(d,p)	17.93(14.47)	−32.26(−31.52)	1.63	4.47	1.93	16.79(12.72) <sup>g</sup> 16.13(12.44) <sup>h</sup>	−31.69(−31.45)	4.95	5.57 <sup>g</sup> 6.05 <sup>h</sup>	1.92		
MRPT2/CASSCF(10,9)/6-31G(d,p)	9.72(6.03) <sup>e</sup>	−18.95(−18.31) <sup>e</sup>				6.02(1.22) <sup>g</sup> 8.36(3.82) <sup>h</sup>	−19.86(−19.63)					
MRPT2/CASSCF(10,9)/6-311G(d,p)	9.28(5.82)	−18.66(−17.92)				5.63(1.56) <sup>g</sup> 10.78(7.09) <sup>h</sup>	−19.22(−18.98)					
B3LYP/6-31G(d,p)	6.79(3.03)	−18.13(−17.64)	4.31	3.09	1.76	5.11(0.12)	−15.31(−14.59)	3.75	3.04	1.53		
CAM-B3LYP/6-31G(d,p)	6.30(2.68)	−19.68(−18.97)	4.17	3.32	1.84	4.52(−0.37)	−16.57(−15.63)	3.68	3.13	1.71		
LC-BLYP/6-31G(d,p)	5.99(2.56)	−19.23(−18.22)	3.67	3.30	2.00	3.74(−0.86)	−16.02(−14.78)	3.20	3.04	1.92		
M062X/6-31G(d,p)	5.26(2.18)	−20.22(−19.21)	4.21	3.40	1.80	2.64(−1.28)	−16.68(−15.63)	3.67	3.18	1.68		
WB97XD/6-31G(d,p)	7.88(4.04)	−19.91(−19.31)	4.24	3.32	1.86	6.32(0.96)	−16.86(−16.20)	3.74	3.17	1.70		
B3LYP/6-311+G(d,p)	9.24(5.24)	−17.62(−17.09)	4.10	3.44	1.42	6.52(2.12)	−15.27(−14.67)	3.84	4.30	1.32		
CAM-B3LYP/6-311+G(d,p)	9.09(5.21)	−18.77(−18.00)	3.87	3.39	1.59	6.26(1.83)	−16.23(−15.42)	3.71	4.12	1.60		
LC-BLYP/6-311+G(d,p)	9.09(5.41)	−17.94(−16.83)	3.23	3.20	1.85	5.84(1.38)	−15.42(−14.33)	3.20	3.64	1.91		
M062X/6-311+G(d,p)	8.28(4.90)	−19.15(−18.26)	3.88	3.33	1.51	5.23(0.76)	−16.72(−15.78)	3.74	3.16	1.60		
WB97XD/6-311+G(d,p)	10.26(6.12)	−19.00(−18.37)	4.01	3.38	1.67	7.77(3.12)	−16.46(−15.66)	3.78	4.26	1.60		

<sup>a</sup> The numbers in parentheses include zero-point energies. <sup>b</sup> Ref 6. <sup>c</sup> Ref 41. <sup>d</sup> Ref 7. <sup>e</sup> Ref 4. <sup>f</sup> Refs 42 and 43. <sup>g</sup> TS1. <sup>h</sup> TS2.

consistent with hydrogen transfer reactions of the heavy–light–heavy mass combinations, where the heavy-atom motions are well separated from the light-atom motions; the heavy atoms rarely move while the hydrogen moves significantly.

**3.2. 1:2 Complex of 7Al with H<sub>2</sub>O in the Gas Phase.** Optimized structural parameters of the reactant, product, and TS in the 7Al–(H<sub>2</sub>O)<sub>2</sub> complexes are listed in Table 2, and structures at the CASSCF/6-31G(d,p) level are depicted in Figure 2. For the 7Al–(H<sub>2</sub>O)<sub>2</sub> cluster, the structural parameters of the reactant obtained from the fit to the rotation constants<sup>16</sup> are also in Table 2. Our CASSCF(10,9) H-bond distances are longer than these values. It is interesting to note that all H-bond distances in the 7Al–(H<sub>2</sub>O)<sub>2</sub> complexes were smaller than those in 7Al–H<sub>2</sub>O complexes. Particularly, all TDDFT methods using the 6-31G(d,p) basis set predicted very short H bonds for the reactant. Short H-bond distance indicates stronger H-bond strength, and linear H bonds are generally stronger than bent H bonds. The H bonds in 7Al–(H<sub>2</sub>O)<sub>2</sub> complexes were more linear and shorter than those of the 7Al–H<sub>2</sub>O complexes. H-bond distances in the reactant, H<sub>10</sub>–O<sub>16</sub>, H<sub>17</sub>–O<sub>20</sub>, and H<sub>19</sub>–N<sub>6</sub> at the B3LYP level, were 0.140 Å, 0.171 Å, and 0.198 Å shorter than the corresponding CASSCF values, respectively (Table 2). In the product, H-bond distances, N<sub>1</sub>–H<sub>10</sub>, O<sub>16</sub>–H<sub>17</sub>, and O<sub>20</sub>–H<sub>19</sub> at the B3LYP level, were 0.241 Å, 0.186 Å, and 0.212 Å shorter than the corresponding CASSCF values. When long-range corrected functionals (CAM-B3LYP) were used, reactant and product H-bond distances became slightly smaller than those from the uncorrected method. The M062X and WB97XD methods also predicted smaller H-bond distances compared with CASSCF results. All TDDFT methods used in this study were found to overestimate H-bond strength in the excited state, although use of the larger basis set could remedy this a little bit. Further studies are necessary to understand the

reliability of the TDDFT methods to predict H-bond strength in the excited state.

The geometry of the TS was fully optimized at the TDDFT and CASSCF(10,9) levels and was confirmed by frequency calculations. Interestingly, two TS structures at the CASSCF(10,9) level were found (Figure 2). In the first TS (denoted as TS1), the H<sub>10</sub> moved more than halfway from N<sub>1</sub> toward the O<sub>16</sub> atom with the H<sub>17</sub> and H<sub>19</sub> rarely moving, which generated a H<sub>3</sub>O<sup>+</sup>-like moiety in a portion of the TS (at O<sub>16</sub>). However, in the second TS (denoted as TS2), the H<sub>19</sub> moved more than halfway from the O<sub>20</sub> to the N<sub>6</sub> atom, but H<sub>10</sub> and H<sub>17</sub> rarely moved, resulting in a HO<sup>−</sup>-like moiety in a portion of the TS (at O<sub>20</sub>). Due to the fact that only one proton moved substantially, while the other two protons moved slightly, a stepwise mechanism with a possible intermediate was predicted. However, every attempt to locate the intermediate led to either the reactant or the product. These results suggest that two concerted but asynchronous processes exist in the ESTPT, one via TS1 and the other via TS2. Very recently, Sakota et al.<sup>17</sup> reported potential energy curves for the ESTPT reaction coordinate in the 7Al–(H<sub>2</sub>O)<sub>2</sub> complex under the assumption of a synchronous process. No potential energy well for an intermediate was found, but the reaction coordinate was not intrinsic, so their argument for a concerted mechanism did not have definitive evidence. Our results are consistent with a concerted mechanism of the ESTPT; however, there are two asynchronous pathways through TS1 and TS2.

We were unable to locate two different TSs at all TDDFT levels used in this study. The bond distances listed at the TDDFT level using the 6-31G(d,p) basis set revealed that the locations of each hydrogen atom at the TS were closer to the center of the two end atoms compared with those from the CASSCF method, and their positions were close to the reactant, satisfying Hammond's postulate.

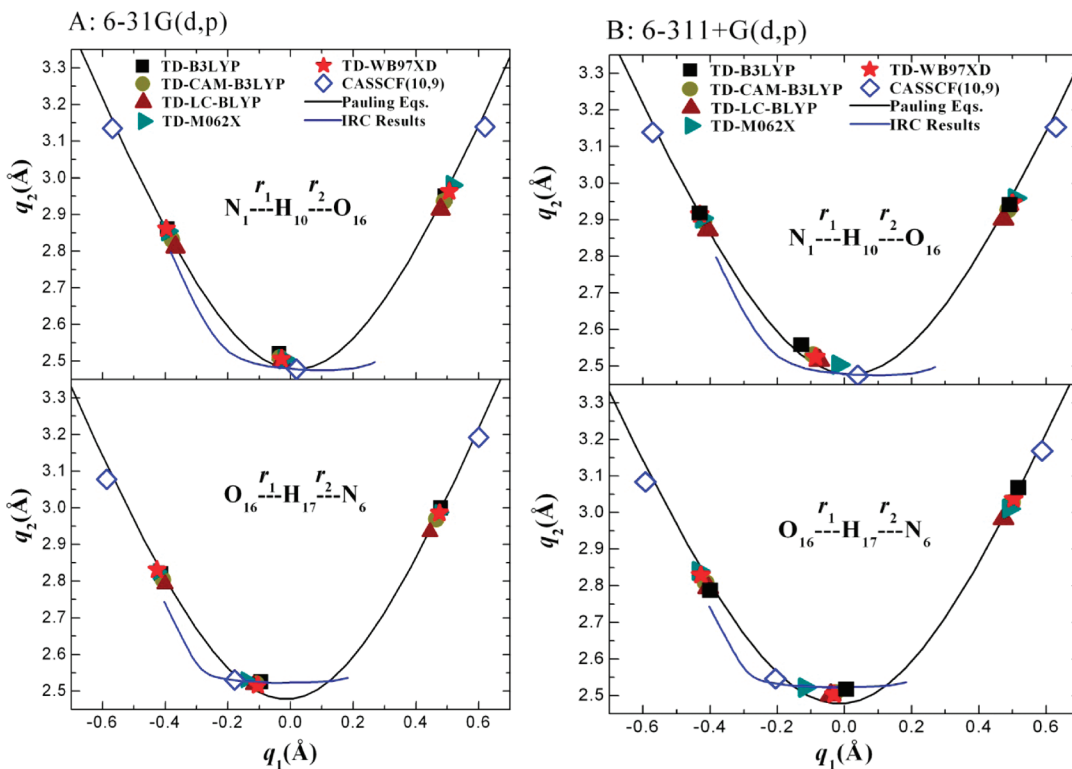


**Figure 3.** Correlation of the H-bond distances  $q_2 = r_1 + r_2$  with the proton transfer coordinate  $q_1 = 1/2(r_1 - r_2)$  for the 7AI–H<sub>2</sub>O complex in the gas phase. Top, H<sub>10</sub> transfer; bottom, H<sub>17</sub> transfer. The black line designates the correlation that satisfies conservation of the bond order. Parameters for Pauling equations were from the literature.<sup>45</sup> The region above and below the black line is where the sum of bond order is smaller and larger than unity, respectively. The correlation points at the bottom near  $q_1 = 0$  are for the TS, and those at the top left and right corners are for the reactant and product, respectively. The blue line represents the correlation along the intrinsic reaction coordinate (IRC) calculated at the CASSCF(10,9)/6-31G(d,p) level. The CASSCF points in B were calculated using the 6-311G(d,p) basis set.

The correlation between  $q_1$  and  $q_2$  for the ESTPT in 7AI–(H<sub>2</sub>O)<sub>2</sub> complexes is depicted in Figure 4. All TDDFT methods predicted smaller  $q_2$  values for the reactant and product than CASSCF, which was attributed to overestimated H-bond strength. The opposite sign of the  $q_1$  values for H<sub>10</sub> and H<sub>19</sub> in TS1 was a clear indication of asynchronicity in the concerted proton transfer. For H<sub>10</sub> transfer, the TS1 and TS2  $q_1$  values at the CASSCF level were very positive and negative, respectively. The  $q_1$  values for H<sub>19</sub> transfer were opposite those for H<sub>10</sub> transfer. These results indicate that the asynchronicity of the two processes (each via TS1 and TS2) is opposite in terms of the order of H<sub>10</sub> and H<sub>19</sub> transfers. It is interesting to note that the correlation points for TS1 and TS2 were under the solid line, which suggests that the total bond order at TS1 and TS2 is not conserved, but increased. The formation of H<sub>3</sub>O<sup>+</sup>-like and HO<sup>-</sup>-like moieties at TS1 and TS2, respectively, might induce coulomb interactions to increase the bond order.

Recently, Limbach et al.<sup>49</sup> has depicted the correlated NHN hydrogen bond coordinates of various systems including the 7AI dimer in the S<sub>1</sub> state. They found that proton transfer is accompanied by a heavy atom motion and the hydrogen bond compression is the most important heavy atom motion. The transition state structures correspond to the strongest possible NHN hydrogen bonds. The double proton transfer in the 7AI dimer occurs stepwise via a zwitterionic intermediate. There are two possible pathways of the stepwise process depending on the order of the H atom in flight, the TSs of which having opposite signs in the  $q_1$  values and smaller  $q_2$  values compared

with those of the reactants. The  $q_1$  and  $q_2$  values of two TSs in the asynchronous and concerted reaction are consistent with those of the stepwise reaction in 7AI dimer.

At TDDFT levels using the 6-31G(d,p) basis set, all TS  $q_1$  values for H<sub>10</sub> and H<sub>19</sub> transfers were in the middle of two points for TS1 and TS2, which were negative but closer to  $q_1 = 0$  (Figure 4). All TS structures using the 6-31G(d,p) basis set resembled the reactant, satisfying Hammond's postulate, and the asynchronicity of the ESTPT was greatly reduced. When the larger 6-311+G(d,p) basis sets were used, all TS correlation points moved toward the TS2 point except for the M062X. Since the  $q_1$  values for H<sub>19</sub> transfer became positive but those for H<sub>10</sub> transfer became more negative, the asynchronicity of the ESTPT was increased again in this case. The TS  $q_1$  values for H<sub>10</sub> and H<sub>19</sub> at the M062X level changed very little and remained approximately in the middle of the TS1 and TS2 points, which were −0.05 and −0.135, respectively. The negative TS  $q_1$  values indicate early TS, satisfying Hammond's postulate.

**3.3. The Energetics of Excited-State Proton Transfer in the Gas Phase.** Barrier heights ( $\Delta V$ ), excited-state tautomerization energies ( $\Delta E$ ), and dipole moments ( $\mu$ ) for the 7AI–H<sub>2</sub>O and 7AI–(H<sub>2</sub>O)<sub>2</sub> complexes are listed in Table 3. Chaban and Gordon<sup>4</sup> calculated the barrier heights in the 7AI–H<sub>2</sub>O complex at the CASSCF(10,9)/DZP and MCQDPT2 levels. They found that the CIS and CASSCF methods overestimated the energy barriers of the excited state and suggested that dynamic electron correlation should be considered. Duong and Kim<sup>42,43</sup> used the CASSCF(10,9)/6-31G(d,p) method followed by single-point

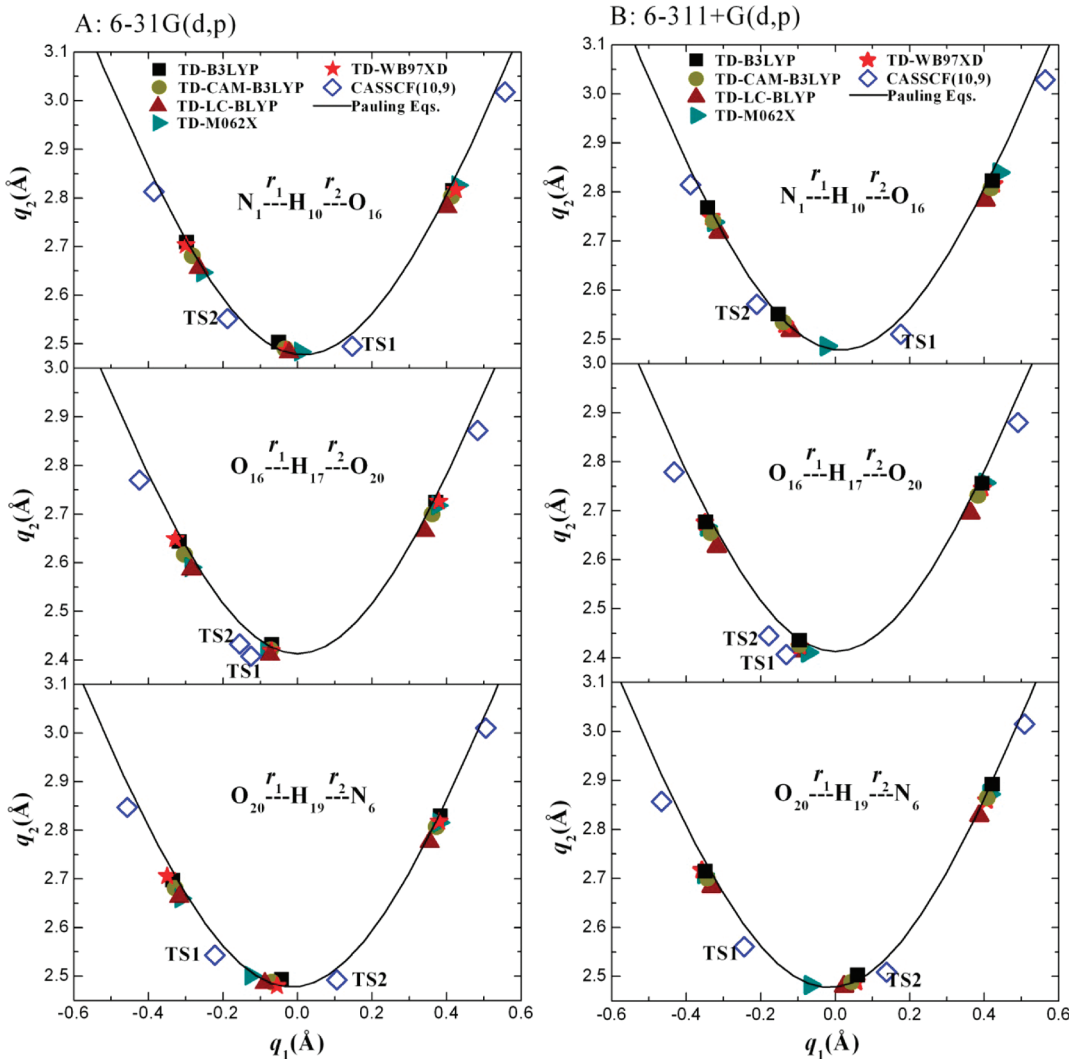


**Figure 4.** Correlation of the H-bond distances  $q_2 = r_1 + r_2$  with the proton transfer coordinate  $q_1 = 1/2(r_1 - r_2)$  for the 7AI- $(\text{H}_2\text{O})_2$  complex in the gas phase. Top,  $\text{H}_{10}$  transfer; middle,  $\text{H}_{17}$  transfer; bottom,  $\text{H}_{19}$  transfer. The solid line represents the correlation for equilibrium distances calculated with Pauling equations. The CASSCF points in B were calculated using the 6-311G(d,p) basis set.

MRPT2 corrections to calculate the ESDPT energetics of the 7AI- $\text{H}_2\text{O}$  complex. The tautomerization energies were  $-18.3$  and  $-19.0$  kcal/mol with and without ZPE corrections, respectively. The  $\Delta E$  values of the 7AI- $(\text{H}_2\text{O})_2$  complex were  $-19.9$  and  $-19.2$  kcal/mol using the 6-31G(d,p) and 6-311G(d,p) basis sets, respectively, without ZPE corrections. The tautomerization energies predicted from the 7AI- $\text{H}_2\text{O}$  and 7AI- $(\text{H}_2\text{O})_2$  complexes agreed well, within 1 kcal/mol.

The MRPT2 barrier height of the excited-state tautomerization in the 7AI- $\text{H}_2\text{O}$  complex was 9.7 and 9.3 kcal/mol using the 6-31G(d,p) and 6-311G(d,p) basis sets, respectively. For the triple proton transfer in the 7AI- $(\text{H}_2\text{O})_2$  complex, two transition states were predicted at the CASSCF levels, and the barrier heights of TS1 and TS2 were 16.8 and 16.1 kcal/mol, respectively, using the 6-311G(d,p) basis set. TS2 was 0.7 kcal/mol lower in barrier height, and 0.3 kcal/mol with ZPE corrections. However, when we included the dynamic electron correlation at the MRPT2 level, the TS1 and TS2 barrier heights were reduced to 5.6 and 10.8 kcal/mol, respectively. It is very interesting that TS1 had an approximately 5.2 kcal/mol lower barrier height than TS2. These results suggest that the triple proton transfer in the

excited state occurred preferably via TS1. The dynamic electron correlation not only reduced barrier heights but also changed the ESTPT mechanism. When the ZPE correction was included using the frequencies calculated at the CASSCF level, the TS1 barrier height was only 1.6 kcal/mol. The difference in the ZPE-corrected barrier height between the 7AI- $\text{H}_2\text{O}$  and 7AI- $(\text{H}_2\text{O})_2$  complexes was 4.2 kcal/mol, using the 6-311G(d,p) basis set at the MRPT2 level. This result supports the argument of Sakota et al. that the gas phase tautomerization in the excited state can occur via a concerted triple proton transfer in the 7AI- $(\text{H}_2\text{O})_2$  complex,<sup>18</sup> although that was not observed in the 7AI- $\text{H}_2\text{O}$  complex.

At the TDDFT level, the excited-state tautomerization energies for the 7AI- $\text{H}_2\text{O}$  complex agreed well with those at the MRPT2 level within 1.4 kcal/mol; however, those for the 7AI- $(\text{H}_2\text{O})_2$  complex gave a maximum deviation of 4.7 kcal/mol compared with the MRPT2 values. Unlike the MRPT2 level, the TDDFT methods could not consistently reproduce the tautomerization energies of the 7AI- $\text{H}_2\text{O}$  and 7AI- $(\text{H}_2\text{O})_2$  complexes. The ZPE-corrected barrier heights for the 7AI- $\text{H}_2\text{O}$  complex obtained by TDDFT methods using the 6-31G(d,p)

**Table 4. Geometric Parameters of Reactant, Product, and Transition States for Excited-State Proton Transfer in 7Al-H<sub>2</sub>O Complexes in Water<sup>a</sup>**

computational method	reactant		product	
	$r(\text{H}_{10}-\text{O}_{16})$	$r(\text{H}_{17}-\text{N}_6)$	$r(\text{N}_1-\text{H}_{10})$	$r(\text{O}_{16}-\text{H}_{17})$
CASSCF(8,8)/6-31G(d) <sup>b</sup>	2.189	2.118	2.168	2.200
CASSCF(10,9)/6-31G(d,p) <sup>c</sup>	2.255	2.098	2.179	2.254
CASSCF(10,9)/6-311G(d,p)	2.284	2.103	2.182	2.282
B3LYP/6-31G(d,p)	1.914	1.840	1.957	2.030
B3LYP/6-311+G(d,p)	2.073	1.833	1.929	2.192
CAM-B3LYP/6-31G(d,p)	1.885	1.837	1.949	1.982
CAM-B3LYP/6-311+G(d,p)	2.023	1.836	1.926	2.104
LC-BLYP/6-31G(d,p)	1.862	1.826	1.925	1.927
LC-BLYP/6-311+G(d,p)	1.982	1.823	1.903	2.025
M062X/6-31G(d,p)	1.908	1.867	2.000	1.994
M062X/6-311+G(d,p)	1.998	1.882	1.985	2.046
WB97XD/6-31G(d,p)	1.916	1.871	1.979	2.006
WB97XD/6-311+G(d,p)	2.046	1.858	1.953	2.101
transition state				
	$r(\text{N}_1-\text{H}_{10})$	$r(\text{H}_{10}-\text{O}_{16})$	$r(\text{O}_{16}-\text{H}_{17})$	$r(\text{H}_{17}-\text{N}_6)$
CASSCF(8,8)/6-31G(d) <sup>b</sup>	1.076	1.580	1.288	1.212
CASSCF(10,9)/6-31G(d,p) <sup>c</sup>	1.352	1.135	1.008	1.671
CASSCF(10,9)/6-311G(d,p)	1.364	1.124	0.996	1.727
B3LYP/6-31G(d,p)	1.242	1.276	1.177	1.348
B3LYP/6-311+G(d,p)	1.052	1.760	1.392	1.157
CAM-B3LYP/6-31G(d,p)	1.262	1.242	1.146	1.379
CAM-B3LYP/6-311+G(d,p)	1.061	1.687	1.397	1.150
LC-BLYP/6-31G(d,p)	1.275	1.221	1.135	1.387
LC-BLYP/6-311+G(d,p)	1.075	1.609	1.405	1.144
M062X/6-31G(d,p)	1.286	1.215	1.105	1.443
M062X/6-311+G(d,p)	1.304	1.198	1.111	1.433
WB97XD/6-31G(d,p)	1.271	1.230	1.140	1.384
WB97XD/6-311+G(d,p)	1.057	1.714	1.403	1.145

<sup>a</sup> Bond distances are in Å. The solvent model is IEFPCM/UFF. Atomic radii from the UFF force field were scaled by 1.1. All hydrogens have individual spheres. <sup>b</sup> The Onsager solvation model was used. Ref 7. <sup>c</sup> Ref 42.

basis set were underestimated by between 1.99 and 3.85 kcal/mol compared with the MRPT2 value. When the 6-311+G(d,p) basis set was used, the TDDFT barriers showed better agreement with the MRPT2 values. However, as discussed previously, the TS structures were utterly dependent on the size of the basis sets. Figure 3 shows that the TS correlation points at the TDDFT level moved further away from the point of CASSCF using larger basis sets; the correlation points of H<sub>10</sub> and H<sub>17</sub> moved toward the reactant and product, respectively. Although the TDDFT barriers using the 6-311+G(d,p) basis set agreed better with the MRPT2 values, they should be used carefully because of their TS structures. As mentioned earlier, only the M062X level gave similar correlations with CASSCF, and the ZPE-corrected barrier using the larger basis sets was 4.9 kcal/mol, which is only 0.9 kcal/mol lower than the MRPT2 value.

Unlike the CASSCF level, only one TS structure was found for the 7Al-(H<sub>2</sub>O)<sub>2</sub> complex at all TDDFT levels used in this study. Figure 4 shows that the TS correlation points of H<sub>10</sub> and H<sub>19</sub> were approximately in the middle of the two TS1 and TS2 points using the 6-31G(d,p) basis set but shifted toward the TS2 point using larger basis sets. Just as the TS structures depend on

the basis sets, so do barrier heights. All TDDFT barriers using the 6-31G(d,p) basis sets, except WB97XD, were underestimated compared with the corresponding MRPT2 value (Table 3). The ZPE-corrected barriers were very small, even smaller than zero in some cases. These barriers became even higher than the MRPT2 value of TS1 in most cases when the larger 6-311+G(d,p) basis set was used. As described above, the TS structures with larger basis sets are more like TS2 rather than TS1 at the CASSCF level, and the MRPT2 barrier of TS2 is much higher. Thus, the structural change of TS toward TS2 seems to increase the barrier heights at the TDDFT level. The correlation points at the M062X level varied very little and remained approximately in the same position in spite of using larger basis sets (Figure 4). The barrier height was 5.23 kcal/mol using the 6-311+G(d,p) basis set, which agreed very well with the MRPT2 value of TS1 using the 6-311G(d,p) basis set (only 0.4 kcal/mol smaller). For both 7Al-H<sub>2</sub>O and 7Al-(H<sub>2</sub>O)<sub>2</sub> complexes, the M062X level reproduced the barrier height quite well using the 6-311+G(d,p) basis set. Because the TS structures and barrier heights from the TDDFT method depend on the basis set size, one should use these methods very carefully, particularly for excited-state proton

**Table 5.** Geometric Parameters of Reactant, Product, and Transition States for Excited-State Proton Transfer in 7AI-(H<sub>2</sub>O)<sub>2</sub> Complexes in Water<sup>a</sup>

computational method	reactant			product		
	<i>r</i> (H <sub>10</sub> -O <sub>16</sub> )	<i>r</i> (O <sub>20</sub> -H <sub>17</sub> )	<i>r</i> (H <sub>19</sub> -N <sub>6</sub> )	<i>r</i> (N <sub>1</sub> -H <sub>10</sub> )	<i>r</i> (O <sub>16</sub> -H <sub>17</sub> )	<i>r</i> (O <sub>20</sub> -H <sub>19</sub> )
CASSCF(8,8)/6-31G(d) <sup>b</sup>	1.992	1.894	2.006	2.060	1.914	2.040
CASSCF(10,9)/6-31G(d,p)	1.818	1.878	1.890	2.062	1.928	2.042
CASSCF(10,9)/6-311G(d,p)	1.825	1.898	1.905	2.071	1.939	2.056
B3LYP/6-31G(d,p)	1.686	1.688	1.699	1.822	1.743	1.818
B3LYP/6-311+G(d,p)	1.770	1.747	1.720	1.827	1.788	1.896
CAM-B3LYP/6-31G(d,p)	1.663	1.664	1.694	1.811	1.716	1.788
CAM-B3LYP/6-311+G(d,p)	1.746	1.723	1.718	1.813	1.758	1.857
LC-BLYP/6-31G(d,p)	1.639	1.629	1.682	1.784	1.674	1.744
LC-BLYP/6-311+G(d,p)	1.721	1.686	1.703	1.782	1.715	1.806
M062X/6-31G(d,p)	1.630	1.653	1.680	1.841	1.738	1.796
M062X/6-311+G(d,p)	1.745	1.753	1.741	1.853	1.788	1.862
WB97XD/6-31G(d,p)	1.685	1.703	1.726	1.831	1.749	1.799
WB97XD/6-311+G(d,p)	1.752	1.750	1.741	1.827	1.780	1.854
transition state						
	<i>r</i> (N <sub>1</sub> -H <sub>10</sub> )	<i>r</i> (H <sub>10</sub> -O <sub>16</sub> )	<i>r</i> (O <sub>16</sub> -H <sub>17</sub> )	<i>r</i> (H <sub>17</sub> -O <sub>20</sub> )	<i>r</i> (O <sub>20</sub> -H <sub>19</sub> )	<i>r</i> (H <sub>19</sub> -N <sub>6</sub> )
CASSCF(8,8)/6-31G(d) <sup>b</sup>	1.043	1.668	1.002	1.563	1.345	1.159
CASSCF(10,9)/6-31G(d,p) TS1	1.642	1.005	1.080	1.330	1.014	1.602
CASSCF(10,9)/6-311G(d,p) TS1	1.681	0.995	1.090	1.308	1.007	1.619
CASSCF(10,9)/6-31G(d,p) TS2	1.035	1.693	0.994	1.580	1.371	1.132
CASSCF(10,9)/6-311G(d,p) TS2	1.030	1.719	0.984	1.620	1.351	1.142
B3LYP/6-31G(d,p)	1.148	1.388	1.130	1.317	1.313	1.195
B3LYP/6-311+G(d,p)	1.080	1.556	1.090	1.376	1.513	1.093
CAM-B3LYP/6-31G(d,p)	1.190	1.309	1.134	1.294	1.247	1.240
CAM-B3LYP/6-311+G(d,p)	1.085	1.523	1.091	1.359	1.480	1.100
LC-BLYP/6-31G(d,p)	1.297	1.185	1.139	1.273	1.134	1.362
LC-BLYP/6-311+G(d,p)	1.099	1.476	1.112	1.313	1.442	1.112
M062X/6-31G(d,p)	1.334	1.158	1.116	1.310	1.092	1.436
M062X/6-311+G(d,p) TS1	1.331	1.159	1.129	1.287	1.126	1.378
M062X/6-311+G(d,p) TS2	1.170	1.339	1.119	1.304	1.296	1.198
WB97XD/6-31G(d,p) TS1	1.314	1.171	1.134	1.288	1.134	1.365
WB97XD/6-31G(d,p) TS2	1.170	1.336	1.129	1.300	1.285	1.204
WB97XD/6-311+G(d,p)	1.092	1.498	1.110	1.323	1.525	1.083

<sup>a</sup> Bond distances are in Å. The solvent model is IEFPCM/UFF. Atomic radii from the UFF force field were scaled by 1.1. All hydrogens have individual spheres. <sup>b</sup> The Onsager solvation model was used. Ref 7.

transfer reactions. No special benefit seemed to be gained from the long-range correction and the empirical dispersion in the TDDFT.

**3.4. Effect of Solvation.** The excited-state protropic tautomerization for 7AI in bulk solvents<sup>2,50–53</sup> implies that solvation plays a key role in proton transfer dynamics. In the gas phase, Chaban and Gordon<sup>4</sup> found that the excited-state proton transfer barrier was reduced to  $\leq 6$  kcal/mol when one water molecule was present. As such, the addition of more than one water molecule should lower the activation energy further, in agreement with the view of Siebrand and co-workers.<sup>54</sup> We performed IEFPCM calculations for the cyclic reactant, TS, and product at the TDDFT and CASSCF levels to understand the solvent effect. The cyclic structures of the reactant, product, and TS in solution were also confirmed by frequency calculations. Some optimized geometrical parameters for 7AI-H<sub>2</sub>O and 7AI-(H<sub>2</sub>O)<sub>2</sub>

complexes in water are listed in Tables 4 and 5, respectively. The correlations between  $q_1$  and  $q_2$  for proton transfer in the 7AI-H<sub>2</sub>O and 7AI-(H<sub>2</sub>O)<sub>2</sub> complexes are depicted in Figures 5 and 6.

The H<sub>10</sub> correlation points moved to the upper left corner along the black line due to the solvent effect for the 7AI-H<sub>2</sub>O reactant, irrespective of the computational level and size of the basis sets. However, those of H<sub>17</sub> were changed in the opposite way at the CASSCF level, but nearly unchanged at the TDDFT level (Figure 5). These results indicate that the H<sub>10</sub>-O<sub>16</sub> and N<sub>6</sub>-H<sub>17</sub> H bonds became longer and shorter, respectively, at the CASSCF level in water. However, at the TDDFT level, the N<sub>6</sub>-H<sub>17</sub> H bond changed very little with a slight increase. In the 7AI-H<sub>2</sub>O product, the H<sub>10</sub> correlation points moved slightly down to the left side due to the solvent effect; however, those of H<sub>17</sub> moved up to the right side. These results suggest that the

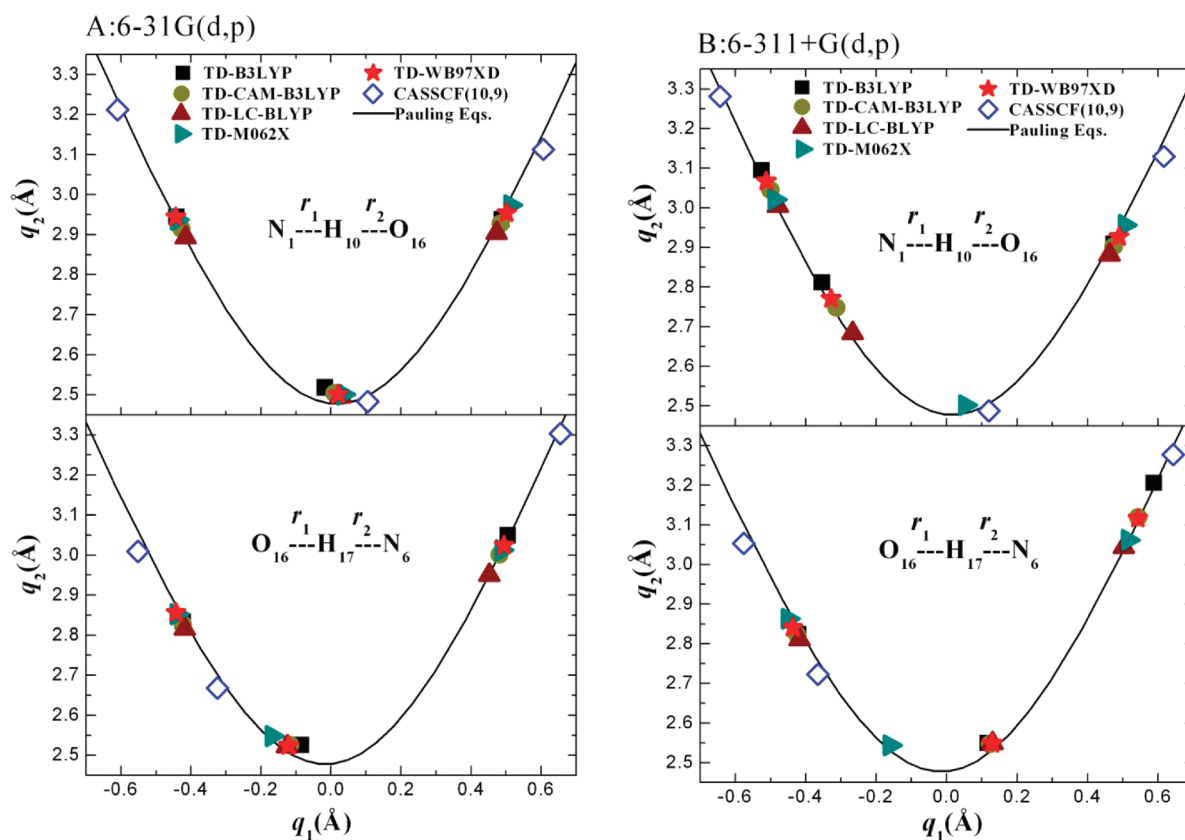


**Figure 5.** Correlation of the H-bond distances  $q_2 = r_1 + r_2$  with the proton transfer coordinate  $q_1 = 1/2(r_1 - r_2)$  for the 7AI–H<sub>2</sub>O complex in water. Top, H<sub>10</sub> transfer; bottom, H<sub>17</sub> transfer. The solid line represents the correlation for equilibrium distances calculated with Pauling equations. The CASSCF points in B were calculated using the 6-311G(d,p) basis set.

N<sub>1</sub>–H<sub>10</sub> and O<sub>16</sub>–H<sub>17</sub> H-bond distances were slightly decreased and increased, respectively, in water. It is interesting to note that at the CASSCF level, two H bonds with a nitrogen atom as an acceptor (N<sub>1</sub>–H<sub>10</sub> in reactant and N<sub>6</sub>–H<sub>17</sub> in product) became shorter in water, whereas those with an oxygen acceptor became longer. These results suggest that the solvent effect could increase the excited-state basicity of the nitrogen atom in 7AI to generate slightly shorter and stronger H bonds.

At the TS, correlation of  $q_1$  with  $q_2$  was dependent on the solvent effect. The H<sub>10</sub> correlation points at the CASSCF level moved slightly to the right side along the Pauling equation line in water; however, those of the H<sub>17</sub> moved to the upper-left side (Figure 5). The differences in  $q_1$  values for H<sub>10</sub> and H<sub>17</sub> transfers increased significantly at the CASSCF level; i.e., the solvent effect greatly increased the asynchronicity of the double proton transfer. At the TDDFT level using the 6-31G(d,p) basis set, the H<sub>10</sub> and H<sub>17</sub>  $q_1$  values became slightly larger and smaller, respectively, in water. However, when the 6-311+G(d,p) basis set was used, the H<sub>10</sub> correlation points at all TDDFT levels except M062X moved greatly toward the upper-left side along the black line in water (Figure 5B), whereas those for H<sub>17</sub> transfer moved to the right side. The difference in  $q_1$  values between H<sub>10</sub> and H<sub>17</sub> transfers increased significantly as well, but in the opposite way compared to that at the CASSCF level. The M062X level showed consistent correlation with the CASSCF level depending on the solvent effect. As a result, the TDDFT methods with the 6-311+G(d,p) basis set, except M062X, predicted completely different asynchronous double proton transfers, where the H<sub>17</sub> atom moved first

followed by the H<sub>10</sub> atom. This mechanism has the opposite order of H transfer when compared with the CASSCF level. Only the M062X level predicted the same mechanism as the CASSCF.

For the 7AI–(H<sub>2</sub>O)<sub>2</sub> reactant at the CASSCF level, the H<sub>10</sub> and H<sub>19</sub> correlation points moved slightly to the upper-left side along the black line in water (Figures 4 and 6); however, those of H<sub>19</sub> rarely moved. For the product, the H<sub>19</sub> correlation points moved slightly to the upper-right side along the solid line, but those of H<sub>10</sub> and H<sub>19</sub> rarely moved. The correlation points for TS depend very much on the solvent effect. As described above, there are two TSs at the CASSCF level for two different ESTPT asynchronous mechanisms. At TS1, the H<sub>10</sub> and H<sub>19</sub> correlation points moved further away toward the right and left side in water, which indicates that the TS positions in terms of the H<sub>10</sub> and H<sub>19</sub> transfers became even more late (product-like) and early (reactant-like), respectively. At TS2, the H<sub>10</sub> and H<sub>19</sub> correlation points moved in the opposite way, which makes the H<sub>10</sub> and H<sub>19</sub> TS positions even earlier and later in water, respectively. These results suggest that the solvent effect increases asynchronicity of the ESTPT for both concerted mechanisms via TS1 and TS2. The H<sub>17</sub> correlation points for TS1 and TS2 were quite close in the gas phase but moved further apart in water; in particular, the TS2 point moved far away to the upper-left side. The position of H<sub>17</sub> at TS2 became very early in water. The increased asynchronicity in water induced the H<sub>3</sub>O<sup>+</sup>-like and OH<sup>−</sup>-like moieties more clearly at TS1 and TS2, respectively. Even in a water solution, we were unable to find an intermediate, and every attempt led to either reactant or product.

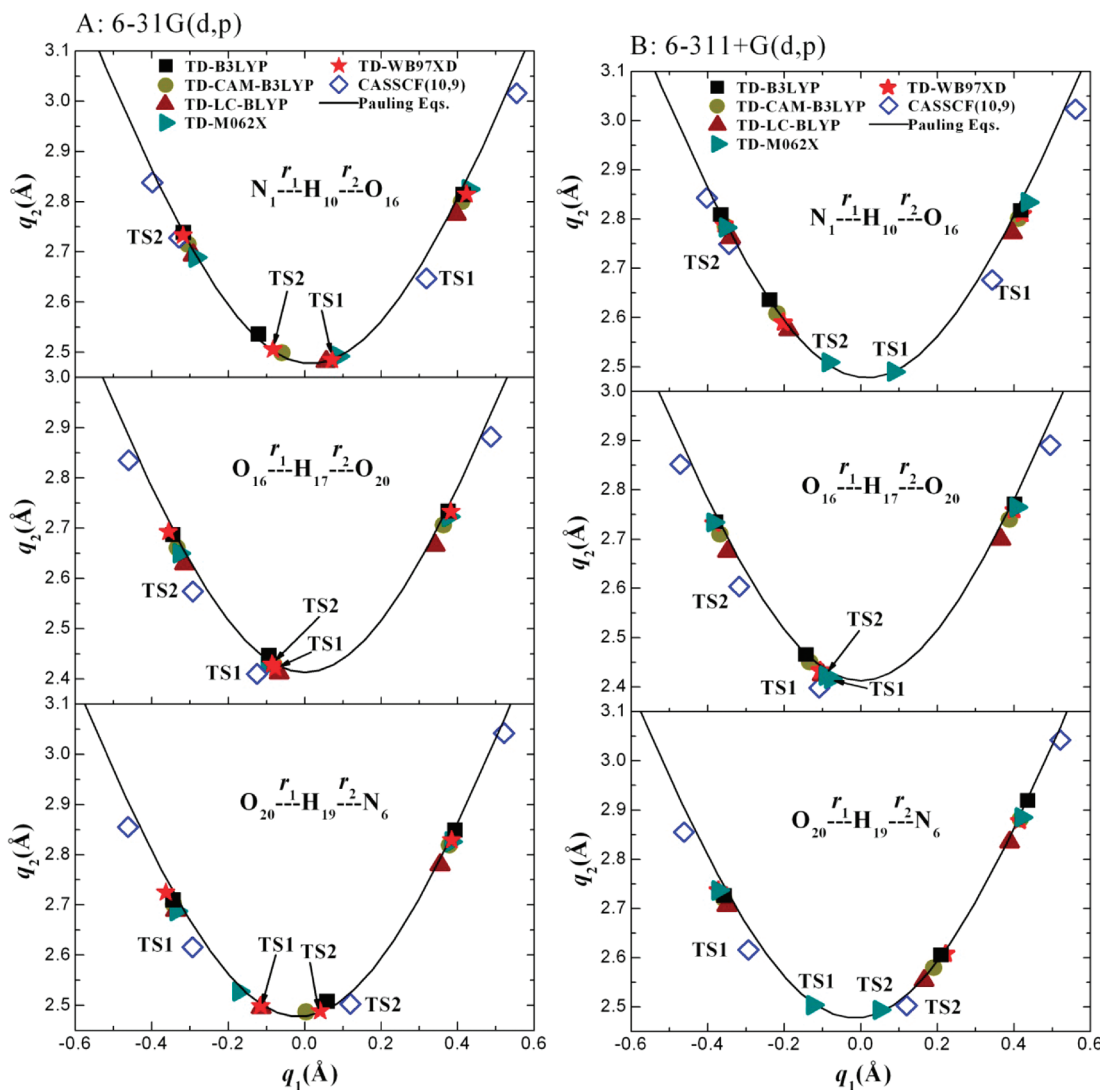


**Figure 6.** Correlation of the H-bond distances  $q_2 = r_1 + r_2$  with the proton transfer coordinate  $q_1 = 1/2(r_1 - r_2)$  for the 7Al- $(\text{H}_2\text{O})_2$  complex in water. Top,  $\text{H}_{10}$  transfer; middle,  $\text{H}_{17}$  transfer; bottom,  $\text{H}_{19}$  transfer. The solid line represents the correlation for equilibrium distances calculated with Pauling equations. The CASSCF points in B were calculated using the 6-311G(d,p) basis set.

No TDDFT level predicted two TSs from two asynchronous paths in the gas phase. However, two TSs were found in water at the WD97XD/6-31G(d,p) and M062X/6-311+G(d,p) levels. As shown in Figure 6, two correlation points for TS1 and TS2 at these two levels were not separated as much as those at the CASSCF level, which implies that the asynchronicity would be predicted as being less.

Unlike the tautomerization energies in the gas phase, the MRPT2 level predicted slightly different energies in water for the 7Al- $\text{H}_2\text{O}$  and 7Al- $(\text{H}_2\text{O})_2$  complexes (Table 6). Tautomerization energy of the 7Al- $\text{H}_2\text{O}$  complex was 4.5 kcal/mol lower (more exoergic) than that of the 7Al- $(\text{H}_2\text{O})_2$  complex at the MRPT2/6-311G(d,p) level, which means that tautomerization in the 7Al- $(\text{H}_2\text{O})_2$  complex is less favorable. The MRPT2 barrier height in the 7Al- $\text{H}_2\text{O}$  complex with ZPE corrections was reduced by 2.8 kcal/mol in aqueous solution, which is consistent with experiments that the excited-state tautomerization was not observed in the gas phase but in solution. In the ESTPT of the 7Al- $(\text{H}_2\text{O})_2$  complex, the MRPT2 barrier for TS1 was 3.9 kcal/mol lower than that for TS2; therefore

tautomerization occurred by a concerted but asynchronous mechanism via TS1. The barrier height for TS1 in water was almost unchanged compared to the value in the gas phase, which indicates that the solvent effect does not give any advantage to the ESTPT in aqueous solution. The MRPT2 barriers of the ESDPT in the 7Al- $\text{H}_2\text{O}$  complex were only 1.4 and 0.8 kcal/mol higher in energy than those of the ESTPT in the 7Al- $(\text{H}_2\text{O})_2$  complex with and without ZPE corrections, respectively. Considering the entropic disadvantage of forming the cyclic TS of three molecules, this energy difference seems to be too small to conclude that the ESTPT instead of the ESDPT is the preferable mechanism of the excited-state tautomerization in aqueous solution at room temperature.

Excited-state dipole moments in the gas phase and in solution are listed in Tables 3 and 6, respectively. The dipole moments of TS are larger than those of reactant at the CASSCF level. For the 7Al- $\text{H}_2\text{O}$  complex, the dipole moment of the reactant and TS forms at the CASSCF(10,9)/6-311G(d,p) level in solution are 2.63 and 7.48 D, while those in the gas phase are 1.63 and 4.47 D, respectively. The changes in geometry upon solvation indicate an

**Table 6.** Reaction Energies, Barrier Heights, and Dipole Moments for the ESPT in 7AI–H<sub>2</sub>O and 7AI–(H<sub>2</sub>O)<sub>2</sub> Complexes in Solution<sup>a</sup>

computational method	7AI–H <sub>2</sub> O						7AI–(H <sub>2</sub> O) <sub>2</sub>					
				$\mu$ (D)						$\mu$ (D)		
	$\Delta V$ (kcal/mol)	$\Delta E$ (kcal/mol)	R	TS	P	$\Delta V$ (kcal/mol)	$\Delta E$ (kcal/mol)	R	TS	P		
CASSCF(8,8)/6-31G(d) <sup>b</sup>	17.94	−33.37	2.47	6.50	2.56	11.61	−32.83	2.07	9.05	3.19		
CASSCF(10,9)/6-31G(d,p) <sup>c</sup>	14.29(12.14)	−31.81(−31.20)	2.65	6.97	2.61	14.66(11.87) <sup>d</sup> 13.21(10.39) <sup>e</sup>	−27.44(−27.78)	7.41	8.81 <sup>d</sup>	2.50	9.84 <sup>e</sup>	
CASSCF(10,9)/6-311G(d,p)	13.48(11.64)	−32.17(−31.54)	2.63	7.48	2.59	15.23(12.79) <sup>d</sup> 13.74(10.83) <sup>e</sup>	−26.57(−26.95)	7.54	9.17 <sup>d</sup>	2.53	9.87 <sup>e</sup>	
MRPT2/CASSCF(10,9)/6-31G(d,p)	5.93(3.78)	−22.20(−21.59)				4.84(2.05) <sup>d</sup> 6.31(3.49) <sup>e</sup>	−15.07(−15.42)					
MRPT2/CASSCF(10,9)/6-311G(d,p)	4.83(2.99)	−18.57(−17.94)				4.07(1.63) <sup>d</sup> 8.39(5.48) <sup>e</sup>	−14.10(−14.48)					
B3LYP/6-31G(d,p)	9.03(4.70)	−15.50(−15.18)	6.04	4.15	2.37	6.19(1.25)	−13.41(−12.88)	5.33	5.64	2.11		
CAM-B3LYP/6-31G(d,p)	8.69(4.58)	−16.14(−15.64)	5.53	4.26	2.39	6.02(0.29)	−13.94(−13.23)	4.88	4.69	2.33		
LC-BLYP/6-31G(d,p)	8.47(4.56)	−14.80(−14.13)	4.69	4.07	2.45	5.33(0.01)	−12.66(−11.80)	3.99	4.07	2.46		
M062X/6-31G(d,p)	7.44(3.98)	−16.61(−16.00)	5.65	4.57	2.32	3.54(−0.38)	−14.13(−13.42)	5.01	4.94	2.24		
WB97XD/6-31G(d,p)	10.38(6.17)	−16.30(−15.76)	5.65	4.31	2.40	7.94(2.18) <sup>d</sup> 7.89(2.38) <sup>e</sup>	−14.14(−13.47)	4.99	4.48 <sup>d</sup>	2.27	5.19 <sup>e</sup>	
B3LYP/6-311+G(d,p)	9.65(6.90)	−14.59(−14.34)	6.09	7.17	2.49	5.40(2.76)	−12.93(−12.56)	5.49	8.51	2.10		
CAM-B3LYP/6-311+G(d,p)	10.26(7.55)	−14.76(−14.26)	5.32	6.72	2.48	5.86(2.98)	−13.08(−12.57)	4.85	7.83	2.36		
LC-BLYP/6-311+G(d,p)	10.96(8.14)	−13.01(−12.42)	4.41	5.78	2.51	6.32(2.83)	−11.48(−10.86)	3.96	6.52	2.50		
M062X/6-311+G(d,p)	10.81(7.29)	−15.12(−14.65)	5.30	4.61	2.26	6.97(2.11) <sup>d</sup> 6.94(1.71) <sup>e</sup>	−13.53(−12.78)	5.06	4.74 <sup>d</sup>	2.24	5.31 <sup>e</sup>	
WB97XD/6-311+G(d,p)	11.37(8.67)	−14.85(−14.46)	5.55	6.99	2.48	7.31(3.98)	−13.22(−12.87)	4.98	7.98	2.30		

<sup>a</sup> The numbers in parentheses include zero-point energies. The solvent model is IEFPCM/UFF. Atomic radii from the UFF force field were scaled by 1.1. All hydrogens have individual spheres. <sup>b</sup> Ref 7. <sup>c</sup> Refs 42 and 43. <sup>d</sup> TS1. <sup>e</sup> TS2.

enhancement of the ionic character of the transition states. The reactant and transition state of the 7AI–(H<sub>2</sub>O)<sub>2</sub> complex, both in the gas phase and in solution at the CASSCF(10,9) level, are more polar than those of 7AI–H<sub>2</sub>O complexes according to their dipole moments. At this level, the differences in dipole moments between the reactant and TS of the cyclic 1:1 complex are much larger than those of the 1:2 complex, which results in a stronger solvent effect to give lower barrier heights in the 1:1 complex, as listed in Tables 3 and 6. It is interesting to note that TS2 is slightly more polar than TS1. TD-DFT predicted excited-state dipole moments in a different way from the CASSCF(10,9) level of theory. The reactant and TS were more and less polar than those at the CASSCF levels, respectively. In addition to that, most TS dipole moments are slightly smaller than reactant dipole moments, except for the 7AI–(H<sub>2</sub>O)<sub>2</sub> complex at the B3LYP, CAM-B3LYP, LC-BLYP, and WB97XD levels using the 6-311+G(d,p) basis sets.

All barrier heights from TDDFT depend on the solvent effect (Table 6). Because most DFT methods with a solvent effect predicted quite different TS structures from those at the CASSCF level, it may not be possible to compare barrier heights from these methods with MRPT2 values. It is interesting to note that most TDDFT barrier heights in water were larger than those in the gas phase, which is opposite of the CASSCF values. Although two asynchronous paths for the 7AI–(H<sub>2</sub>O)<sub>2</sub> complex were found at the WB97XD/6-31G(d,p) and M062X/6-311+G(d,p) levels in water, there was no difference in the barrier heights between the two paths at both levels. These TDDFT

levels failed to distinguish one preferable path from the other. In addition, the barrier heights from the WB97XD/6-31G(d,p) and M062X/6-311+G(d,p) methods were 3.9 and 2.9 kcal/mol larger than the MRPT2 value of the preferable path, respectively. Further systematic study is necessary to test whether current TDDFT methods including solvent effects can be used to understand excited-state proton transfer reactions.

#### 4. CONCLUSIONS

In the present work, systematic investigations on tautomerization processes were performed on 7AI–(H<sub>2</sub>O)<sub>n</sub> (*n* = 1, 2) complexes using TDDFT and CASSCF methods. Complete geometry optimization in the gas phase and in solution was performed in the S<sub>1</sub> state. Comparisons between the TDDFT results and CASSCF values were made carefully. The key conclusions are summarized as follows.

The dynamic electron correction is very important to the energetics of the excited-state tautomerization in 7AI–(H<sub>2</sub>O)<sub>n</sub> (*n* = 1, 2) complexes.

For the 7AI–(H<sub>2</sub>O)<sub>2</sub> complex, CASSCF levels predicted two concerted but asynchronous paths of proton transfer in the excited-state tautomerization: one where the proton from the pyrole ring of 7AI moved first to water and the other where the water proton moved first to the pyridine ring. Because of the asynchronous motion of protons, the H<sub>3</sub>O<sup>+</sup>-like and HO<sup>−</sup>-like moieties were generated in the TS of the former and the latter, respectively. No difference was found between the barrier heights

of the two paths without considering the dynamic electron correlation. However, the MRPT2 correction clearly showed that the former path was much preferable to the latter.

In the gas phase, the barrier of the 7Al-(H<sub>2</sub>O)<sub>2</sub> complex was 1.6 kcal/mol, which is much lower than that of the 7Al-H<sub>2</sub>O complex, supporting the argument that excited-state tautomerization might occur by forming H-bonded complexes with two water molecules. The solvent effect reduced the 7Al-H<sub>2</sub>O MRPT2 barrier by 2.8 kcal/mol, which is consistent with experiments in that the excited-state tautomerization was not observed in the gas phase but in solution.

All DFT methods used in this study, namely, the hybrid functional B3LYP, M062X, the functional with long-range correction CAM-B3LYP, LC-BLYP, and the WB97XD functional which includes empirical dispersion, underestimated H-bond distances in the reactant and product by about 0.1–0.4 Å. The tautomerization energies obtained by the TDDFT methods were slightly underestimated compared with the MRPT2 values, except for the 7Al-H<sub>2</sub>O complex in the gas phase. No significant benefits, in terms of both structural and energetic prediction, were found from the DFT methods with long-range correction or empirical dispersion. In terms of the TS structures and the barrier height in the gas phase, the M062X method agreed best with the CASSCF with a MRPT2 correction.

At all TDDFT levels used in this study, the TS structures and barrier heights greatly depend on the basis set and the solvent effect. Only two methods, WB97XD/6-31G(d,p) and M062X/6-311+G(d,p), predicted two TSs for two asynchronous paths for the 7Al-(H<sub>2</sub>O)<sub>2</sub> complex. However, the two barrier heights were almost the same in energy, and larger than the preferable MRPT2 value. Further systematic study is necessary to test whether current TDDFT methods, including solvent effects, can be used to correctly understand excited-state proton transfer reactions.

## ■ ASSOCIATED CONTENT

**Supporting Information.** Geometric parameters of reactant, product, and transition states. This material is available free of charge via the Internet at <http://pubs.acs.org>.

## ■ AUTHOR INFORMATION

### Corresponding Author

\*E-mail: yhkim@khu.ac.kr

## ■ ACKNOWLEDGMENT

This work was supported by a grant from Kyung Hee University in 2010. We are pleased to acknowledge the support of the Center for Academic Computing at Kyung Hee University for the computing resources.

## ■ REFERENCES

- (1) Miyazaki, T. *Atom Tunneling Phenomena in Physics, Chemistry, and Biology*; Miyazaki, T., Ed.; Springer: Berlin, 2004; pp 1–375.
- (2) Taylor, C. A.; El-Bayoumi, M. A.; Kasha, M. *Proc. Nat. Acad. Sci.* **1969**, *63*, 253–260.
- (3) Gordon, M. S. *J. Phys. Chem.* **1996**, *100*, 3974–3979.
- (4) Chaban, M. G.; Gordon, M. S. *J. Phys. Chem. A* **1999**, *103*, 185–189.
- (5) Nakano, H. *J. Chem. Phys.* **1993**, *99*, 7983–7992.
- (6) Casadesús, R.; Moreno, M.; Lluch, J. M. *Chem. Phys.* **2003**, *290*, 319–336.
- (7) Fernandez-Ramos, A.; Smedarchina, Z.; Siebrand, W.; Zgierski, M. Z. *J. Chem. Phys.* **2001**, *114*, 7518–7526.
- (8) Kina, D.; Nakayama, A.; Noro, T.; Taketsugu, T.; Gordon, M. S. *J. Phys. Chem. A* **2008**, *112*, 9675–9683.
- (9) Chapman, C. F.; Maroncelli, M. *J. Phys. Chem.* **1992**, *96*, 8430–8441.
- (10) Chen, Y.; Gai, F.; Petrich, J. W. *J. Am. Chem. Soc.* **1993**, *115*, 10158–10166.
- (11) Chou, P.-T.; Martinez, M. L.; Cooper, W. C.; McMorrow, D.; Collins, S. T.; Kasha, M. *J. Phys. Chem.* **1992**, *96*, 5203–5205.
- (12) Huang, Y.; Arnold, S.; Sulkes, M. *J. Phys. Chem.* **1996**, *100*, 4734–4738.
- (13) Folmer, D. E.; Wisniewski, E. S.; Stairs, J. R.; Castleman, A. W., Jr. *J. Phys. Chem. A* **2000**, *104*, 10545–10549.
- (14) Nakajima, A.; Hirano, M.; Hasumi, R.; Kaya, K.; Watanabe, H.; Carter, C.; Williamson, J. M.; Miller, T. A. *J. Phys. Chem. A* **1997**, *101*, 392–398.
- (15) Hara, A.; Sakota, K.; Sekiya, H. *Chem. Phys. Lett.* **2005**, *407*, 30–34.
- (16) Vu, T. B. C.; Kalkman, I.; Meerts, W. L.; Svartsov, Y. N.; Jacoby, C.; Schmitt, M. *J. Chem. Phys.* **2008**, *128*, 214311–8.
- (17) Sakota, K.; Jouvet, C.; Dedonder, C.; Fujii, M.; Sekiya, H. *J. Phys. Chem. A* **2010**, *114*, 11161–11166.
- (18) Yokoyama, H.; Watanabe, H.; Omi, T.; Ishiuchi, S.; Fujii, M. *J. Phys. Chem. A* **2001**, *105*, 9366–9374.
- (19) Casida, M. E.; Chong, D. P. *Recent Advances In Density Functional Methods: Part I*; Chong, D. P., Ed.; World Scientific: Singapore, 1995; Chapter 5, pp 155–192.
- (20) Dreuw, A.; Head-Gordon, M. *Chem. Rev.* **2005**, *105*, 4009–4037.
- (21) Dierksen, M.; Grimme, S. *J. Chem. Phys.* **2004**, *120*, 3544–3554.
- (22) Dierksen, M.; Grimme, S. *J. Phys. Chem. A* **2004**, *108*, 10225–10237.
- (23) Van Leeuwen, R.; Baerends, E. J. *Phys. Rev. A* **1994**, *49*, 2421–2431.
- (24) Cave, R. J.; Zhang, F.; Maitra, N. T.; Burke, K. *Chem. Phys. Lett.* **2004**, *389*, 39–42.
- (25) Maitra, N. T.; Zhang, F.; Cave, R. J.; Burke, K. *J. Chem. Phys.* **2004**, *120*, 5932–5937.
- (26) Starcke, J. H.; Wormit, M.; Schirmer, J.; Dreuw, A. *Chem. Phys.* **2006**, *329*, 39–42.
- (27) Tozer, D. J.; Amos, R. D.; Handy, N. C.; Roos, B. J.; Serrano-Andres, L. *Mol. Phys.* **1999**, *97*, 859–868.
- (28) Dreuw, A.; Weisman, J. L.; Head-Gordon, M. *J. Chem. Phys.* **2003**, *119*, 2943–2946.
- (29) Sobolewski, A. L.; Domcke, W. *Chem. Phys.* **2003**, *294*, 73–83.
- (30) Dreuw, A.; Head-Gordon, M. *J. Am. Chem. Soc.* **2004**, *126*, 4007–4016.
- (31) Frisch, M. J.; Truck, G. W.; Schlegel, H. B.; Scuseria, G. E.; Robb, M. A.; Cheeseman, J. R.; Scalmani, G.; Barone, V.; Mennucci, B.; Petersson, G. A.; Nakatsuji, H.; Caricato, M.; Li, X.; Hratchian, H. P.; Izmaylov, A. F.; Bloino, J.; Zheng, G.; Sonnenberg, J. L.; Hada, M.; Ehara, M.; Toyota, K.; Fukuda, R.; Hasegawa, J.; Ishida, M.; Nakajima, T.; Honda, Y.; Kitao, O.; Nakai, H.; Vreven, T.; Montgomery, J. A., Jr.; Peralta, J. E.; Ogliaro, F.; Bearpark, M.; Heyd, J. J.; Brothers, E.; Kudin, K. N.; Staroverov, V. N.; Kobayashi, R.; Normand, J.; Raghavachari, K.; Rendell, A.; Burant, J. C.; Iyengar, S. S.; Tomasi, J.; Cossi, M.; Rega, N.; Millam, J. M.; Klene, M.; Knox, J. E.; Cross, J. B.; Bakken, V.; Adamo, C.; Jaramillo, J.; Gomperts, R.; Stratmann, R. E.; Yazyev, O.; Austin, A. J.; Cammi, R.; Pomelli, C.; Ochterski, J. W.; Martin, R. L.; Morokuma, K.; Zakrzewski, V. G.; Voth, G. A.; Salvador, P.; Dannenberg, J. J.; Dapprich, S.; Daniels, A. D.; Farkas, O.; Foresman, J. B.; Ortiz, J. V.; Cioslowski, J.; Fox, D. J. *Gaussian 09*; Gaussian, Inc.: Wallingford, CT, 2009.
- (32) Schmidt, M. W.; Baldridge, K. K.; Boatz, J. A.; Elbert, S. T.; Gordon, M. S.; Jensen, J. H.; Koseki, S.; Matsunaga, N.; Nguyen, K. A.;

- Su, S. J.; Windus, T. L.; Dupuis, M.; Montgomery, J. A. *J. Comput. Chem.* **1993**, *14*, 1347–1363.  
(33) Furche, F.; Ahlrichs, R. *J. Chem. Phys.* **2002**, *117*, 7433–7447.  
(34) Becke, A. D. *J. Chem. Phys.* **1993**, *98*, 5648–5652.  
(35) Yanai, T.; Tew, D.; Handy, N. *Chem. Phys. Lett.* **2004**, *393*, 51–57.  
(36) Iikura, H.; Tsuneda, T.; Yanai, T.; Hirao, K. *J. Chem. Phys.* **2001**, *115*, 3540–3544.  
(37) Zhao, Y.; Truhlar, D. G. *Theor. Chem. Acc.* **2008**, *120*, 215–241.  
(38) Cancès, E.; Mennucci, B.; Tomasi, J. *Chem. Phys.* **1997**, *107*, 3032–3041.  
(39) Cossi, M.; Barone, V.; Mennucci, B.; Tomasi, J. *Chem. Phys. Lett.* **1998**, *286*, 253–260.  
(40) Mennucci, B.; Tomasi, J. *J. Chem. Phys.* **1997**, *106*, 5151–5158.  
(41) Svartsov, Y. N.; Schmitt, M. *J. Chem. Phys.* **2008**, *128*, 214310–9.  
(42) Duong, M. P. T.; Kim, Y. H. *J. Phys. Chem. A* **2010**, *114*, 3403–3410.  
(43) Duong, M. P. T.; Park, K. S; Kim, Y. H. *J. Photochem. Photobiol. A: Chem.* **2010**, *214*, 100–107.  
(44) Limbach, H. H.; Pietrzak, M.; Benedict, H.; Tolstoy, P. M.; Golubev, N. S.; Denisov, G. S. *J. Mol. Struct.* **2004**, *706*, 115–119.  
(45) Limbach, H. H.; Lopez, J. M.; Kohen, A. *Phil. Trans. R. Soc. London, Ser. B* **2006**, *361*, 1399–1415.  
(46) Limbach, H. H. In *Hydrogen-Transfer Reactions*; Schowen, R. L., Klinman, J. P., Hynes, J. T., Limbach, H. H., Eds; Wiley: Weinheim, Germany, 2007; Chapter 6, pp 135–221.  
(47) Garrett, B. C.; Truhlar, D. G. *J. Am. Chem. Soc.* **1979**, *101*, 4534–4548.  
(48) Johnston, H. S. *Gas Phase Reaction Rate Theory*; Ronald Press: New York, 1966; pp 1–362.  
(49) Lopez, J. M.; Männle, F.; Wawer, I.; Buntkowsky, G.; Limbach, H. H. *Phys. Chem. Chem. Phys.* **2007**, *9*, 4498–4513.  
(50) McMorrow, D.; Aartsma, T. *Chem. Phys. Lett.* **1986**, *125*, 581–585.  
(51) Krijnenberg, J.; Huizer, A. H.; Varma, C. A. G. O. *J. Chem. Soc., Faraday Trans. II* **1988**, *84*, 1163–1175.  
(52) Moog, R. S.; Maroncelli, M. *J. Phys. Chem.* **1991**, *95*, 10359–10369.  
(53) Smirnov, A. V.; English, D. S.; Rich, R. L.; Lane, J.; Teyton, L.; Schwabacher, A. W.; Luo, S.; Thornburg, R. W.; Petrich, J. W. *J. Phys. Chem. B* **1997**, *101*, 2758–2769.  
(54) Smedarchina, Z.; Siebrand, W.; Fernandez-Ramos, A.; Gorb, L.; Leszczynski, J. *J. Chem. Phys.* **2000**, *112*, 566–573.